LA-UR- 11-03210

Approved for public release;
distribution is unlimited.

Title: Models for the Large Plastic Deformation Response of Polycrystalline Metals

Author(s): C. A. Bronkhorst
B. L. Hansen
M. R. Tonks
D. J. Luscher
A. R. Ross
E. K. Cerreta
J. F. Bingert

Intended for: Workshop on Uncertainty Quantification and Multiscale Materials Modeling, Santa Fe, 13-15 June, 2011.

Los Alamos
NATIONAL LABORATORY
EST. 1943

Models for the Large Plastic Deformation Response of Polycrystalline Metals

C. A. Bronkhorst[1], B. L. Hansen[1], M. R. Tonks[3], D. J. Luscher[1],
A. R. Ross[2], E. K. Cerreta[2], J. F. Bingert[2]

[1]Theoretical Division, Fluid Dynamics and Solid Mechanics
[2]Material Science and Technology Division, Radiation & Dynamic Extremes
Los Alamos National Laboratory
Los Alamos, NM

[3]Fuel Modeling and Simulation
Idaho National Laboratory
Idaho Falls, ID

ABSTRACT

The large deformation dynamic response of tantalum has been studied over recent years using crystal plasticity based models. These models represent the morphological features of the microstructure and track the effect of crystallographic orientation on the plastic deformation response of the material. The large deformation shear response of tantalum has been examined using crystal plasticity finite element (CPFE) tools to track the evolution of the microstructure for the imposed dynamic loading profile. With this technique, the microstructure is represented explicitly under two-dimensional axi-symmetric conditions and so grain to grain mechanical interactions are represented. A model for the dynamic single crystal response of the material is presented and the process by which material parameters evaluated is described. Simulations of forced shear experiments are presented and results compared with experimental load/deformation, crystallographic texture, and quantitative metallographic analysis of the deformed shear section. This CPFE technique was also used to motivate a statistically based stochastic Taylor model where a statistical distribution in the driving velocity gradient is employed. In a Taylor model of a polycrystalline material, a velocity gradient is imposed on each grain of the aggregate and the aggregate stress response is the numerical average response of all the grains. Within the Taylor treatment, grain to grain interactions are not accounted for. A similar single crystal model was used in the Taylor model and numerical results are compared against results of Taylor anvil experiments (shape and crystallographic texture of the deformed sample). The talk is concluded by a discussion of where improvements need to be made in the polycrystal modeling representation of large deformation and damage processes in polycrystalline metallic materials. Some brief examples of these future directions are presented.

LA-UR 11-02780

Models for the Large Plastic Deformation Response of Polycrystalline Metals

C. A. Bronkhorst, B. L. Hansen, M. R. Tonks, D. J. Luscher
Theoretical Division

A. R. Ross, E. K. Cerreta, J. F. Bingert
Materials Science & Technology Division

Los Alamos National Laboratory

Workshop on Uncertainty Quantification and Multiscale Materials Modeling
Santa Fe, NM
13-15 June, 2011

Los Alamos

Outline

- Motivation and challenge
- Macro-scale experiments
- Continuum isotropic constitutive model
  - Anisotropic MTS
- Thermo-viscoplastic single crystal model
  - Thermally activated slip
- Embedded polycrystal forced shear simulations
- Comparison to experimental results
- Summary & comments

Los Alamos

Explosively Loaded Sample Demonstrates Ductile Damage and Failure Physics

T. Mason

Explosively Loaded Tantalum Experiment
6 mm thick PETN Beneath Sample – Center Detonated
Soft Sample Recovery

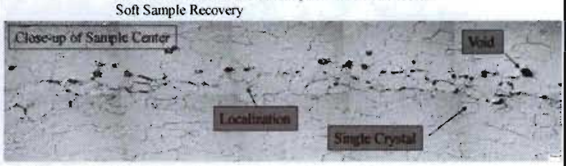

'Void sheets' are forming along grain boundaries in sample

Los Alamos

Challenge of linking microstructure to performance

Ta Plate Impact

B. Henrie

Cu Plane Strain Compression

Undeformed $\varepsilon = -1.5$

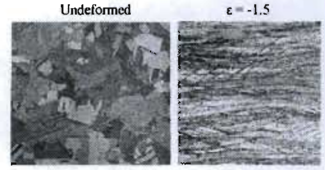

- The ductile failure process generally involves localization, porosity initiation, porosity growth, and coalescence dominated by localized deformation.
- These events occur at the length scale of the single crystal.

Los Alamos

Forced shear experiments

- Axisymmetric, Split-Hopkinson
- Top-to-bottom loading, 10-25 m/s
- Tantalum plate, residual texture (Chen & Gray, 1996; Maudlin et al., 1999), grain size 42 μm
- -100 °C and 25 °C

Dimensions in mm

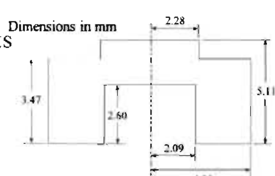

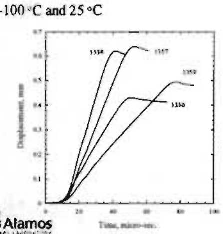

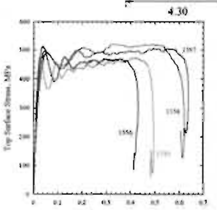

Los Alamos

Numerical model with boundary conditions

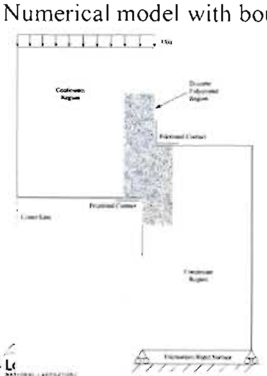

- Axisymmetric, 3 node linear elements for shear zone
- Adiabatic
- Embedded 1091 grain polycrystal region
- 40 μm grain size
- ~ 7 μm element size
- Rate-dependent isotropic continuum regions
- Frictionless contact surfaces at corners
- ABAQUS - implicit used but dynamic displacement rate applied
- 3 crystallographic realizations

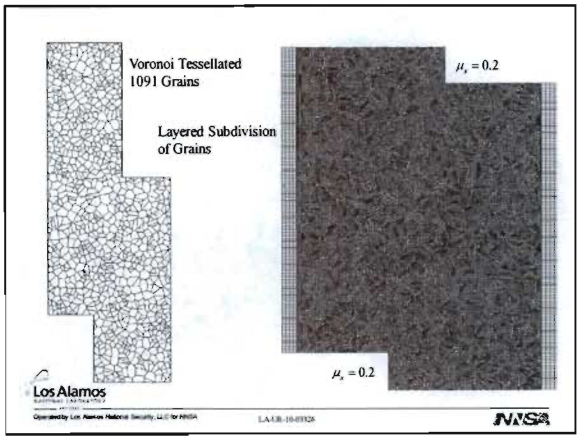
Voronoi Tessellated
1091 Grains
Layered Subdivision
of Grains
$\mu_s = 0.2$
$\mu_s = 0.2$
Los Alamos

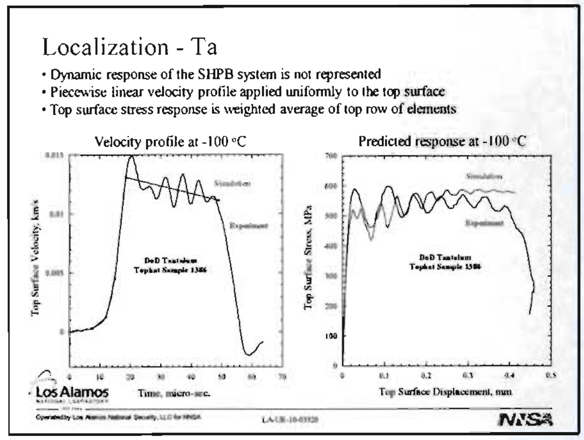
Localization - Ta
• Dynamic response of the SHPB system is not represented
• Piecewise linear velocity profile applied uniformly to the top surface
• Top surface stress response is weighted average of top row of elements
Velocity profile at -100 °C
Predicted response at -100 °C
Simulation
Experiment
Top Surface Velocity, km/s
Time, micro-sec.
Top Surface Stress, MPa
Top Surface Displacement, mm
Los Alamos

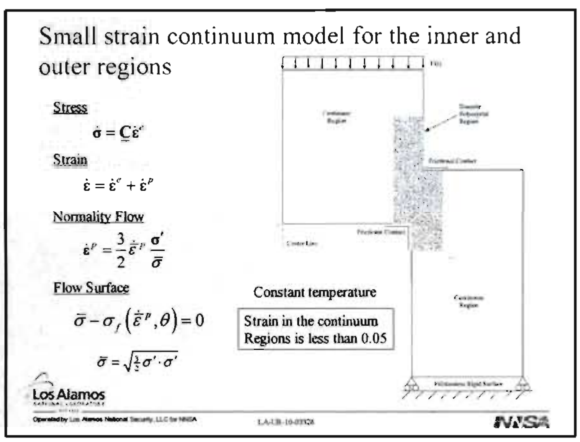
Small strain continuum model for the inner and outer regions
Stress
$\dot{\sigma} = \underline{C}\dot{\varepsilon}^e$
Strain
$\dot{\varepsilon} = \dot{\varepsilon}^e + \dot{\varepsilon}^p$
Normality Flow
$\dot{\varepsilon}^p = \frac{3}{2}\dot{\bar{\varepsilon}}^p \frac{\sigma'}{\bar{\sigma}}$
Flow Surface
$\bar{\sigma} - \sigma_f(\dot{\bar{\varepsilon}}^p, \theta) = 0$
$\bar{\sigma} = \sqrt{\frac{3}{2}\sigma' \cdot \sigma'}$
Constant temperature
Strain in the continuum
Regions is less than 0.05
Los Alamos

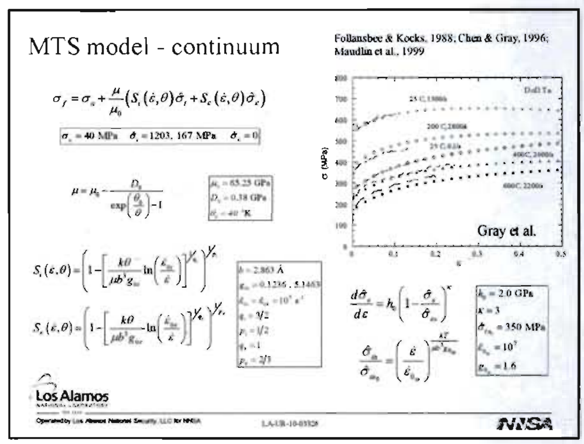
MTS model - continuum
Follansbee & Kocks, 1988; Chen & Gray, 1996; Maudlin et al., 1999
Gray et al.
Los Alamos

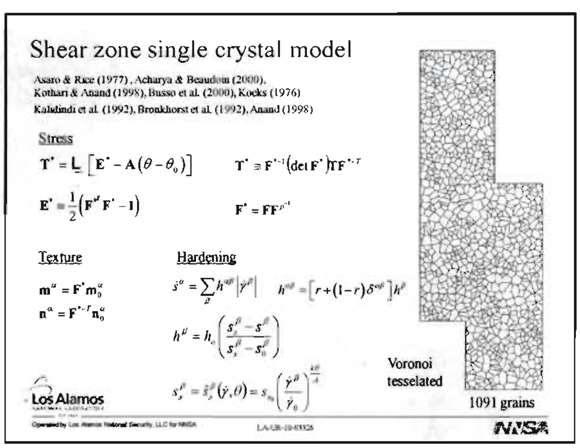
Shear zone single crystal model
Asaro & Rice (1977), Acharya & Beaudoin (2000), Kothari & Anand (1998), Busso et al. (2000), Kocks (1976) Kalidindi et al. (1992), Bronkhorst et al. (1992), Anand (1998)
Stress
Texture
Hardening
Voronoi
tesselated
1091 grains
Los Alamos

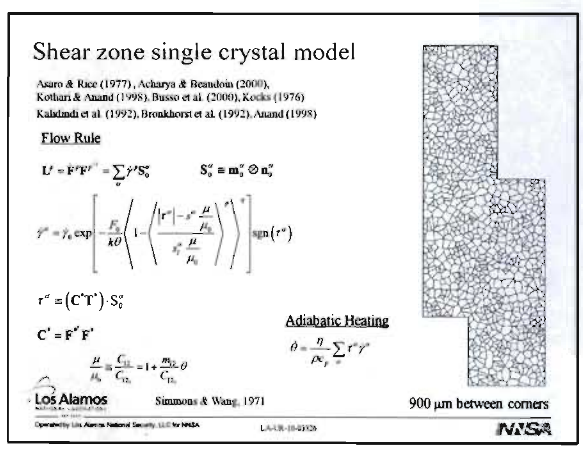
Shear zone single crystal model
Asaro & Rice (1977), Acharya & Beaudoin (2000), Kothari & Anand (1998), Busso et al. (2000), Kocks (1976) Kalidindi et al. (1992), Bronkhorst et al. (1992), Anand (1998)
Flow Rule
Adiabatic Heating
Simmons & Wang, 1971
900 μm between corners
Los Alamos

Single crystal model - Ta

Material Parameter Evaluation
512 Elements/Grains

Single Crystal Model

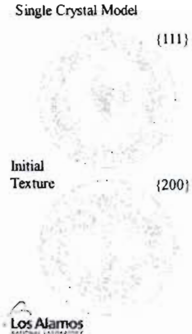

$\rho = 16640$ kg/m^3
$c_p = 150$ J/kg-K
$\alpha = 6.5$ μm/m-K
$\eta = 0.0, 0.95$
$m_{11} = -24.5$ MPa/K
$C_{11} = 268.5$ GPa
$m_{12} = -11.8$ MPa/K
$C_{12} = 159.9$ GPa
$m_{44} = -14.9$ MPa/K
$C_{44} = 87.1$ GPa
$r = 1.4$
$\dot{\gamma}_0 = 10^7$ sec^{-1}
$s_0 = 50$ MPa
$s_I = 550$ MPa
$F_0 = 2.1 \times 10^{-19}$ J
$p = 0.34$
$q = 1.66$
$s_{\epsilon} = 125$ MPa
$h_0 = 300$ MPa
$A = 10^{-15}$ J

Ta - 24 BCC systems
{110}<111>, {112}<111>

Single crystal model - Ta

Single Crystal Model

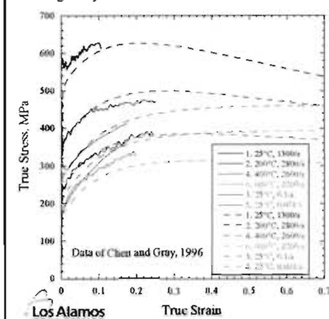

Material Parameter Evaluation

Ta - 24 BCC systems
{110}<111>, {112}<111>

$\rho = 16640$ kg/m^3	$r = 1.4$
$c_p = 150$ J/kg-K	$\dot{\gamma}_0 = 10^7$ sec^{-1}
$\alpha = 6.5$ μm/m-K	$s_0 = 50$ MPa
$\eta = 0.0, 0.95$	$s_I = 550$ MPa
$m_{11} = -24.5$ MPa/K	$F_0 = 2.1 \times 10^{-19}$ J
$C_{11} = 268.5$ GPa	$p = 0.34$
$m_{12} = -11.8$ MPa/K	$q = 1.66$
$C_{12} = 159.9$ GPa	$s_{\epsilon} = 125$ MPa
$m_{44} = -14.9$ MPa/K	$h_0 = 300$ MPa
$C_{44} = 87.1$ GPa	$A = 10^{-18}$ J

Experimental load-displacement response is over-predicted

- Although the loading rate difference is described, overall the model over-predicts the magnitude of load required to deform the sample.
- This is believed to be caused primarily by 2D representation.
- The single crystal model could also be inadequate to well represent this level of detail.

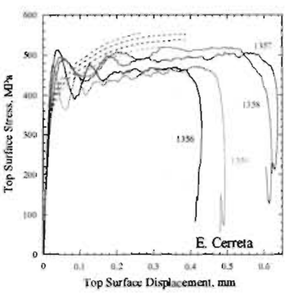

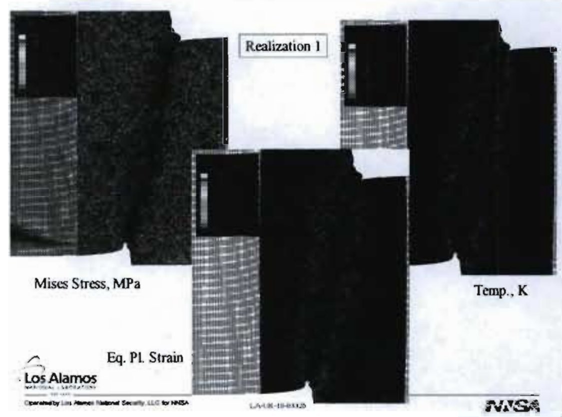

Localization - Ta

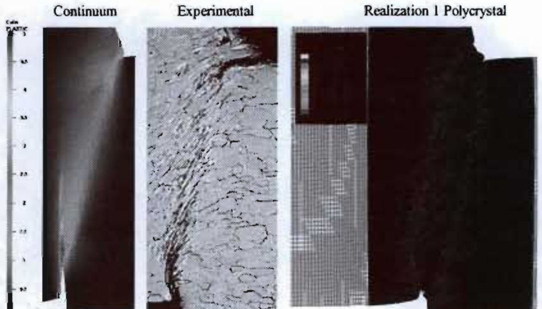

Portion of the shear zone isolated for closer examination.

Statistics of material state
- von Mises stress
- Plastic strain
- Temperature
- Plastic strain rate

Comparison to measurement
- Crystallographic texture
- Strain profile by metallography

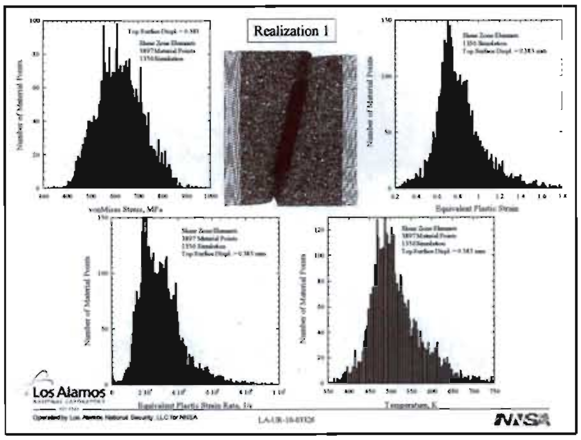
Realization 1
Los Alamos
Operated by Los Alamos National Security, LLC for NNSA
NNSA

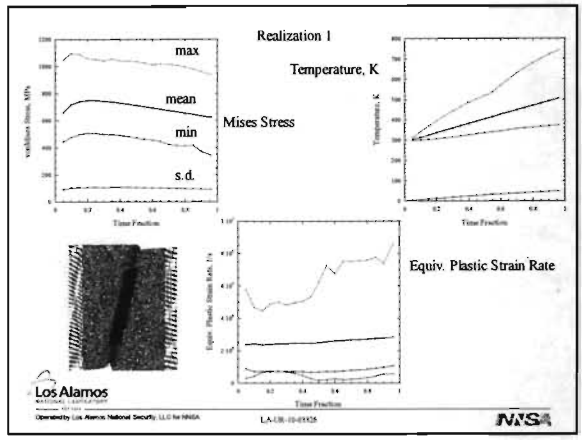
Realization 1
max
mean
min
s.d.
Mises Stress
Temperature, K
Equiv. Plastic Strain Rate
Los Alamos
Operated by Los Alamos National Security, LLC for NNSA
NNSA

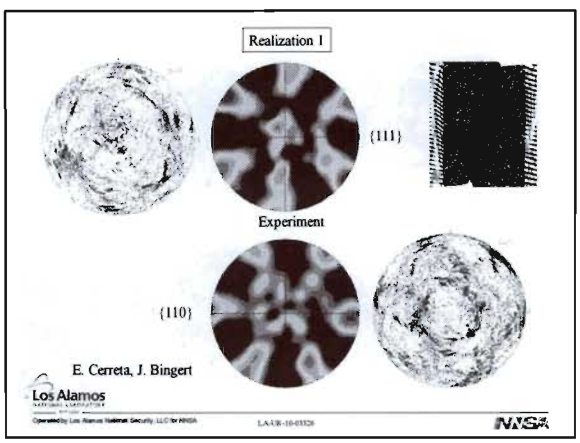
Realization 1
{111}
Experiment
{110}
E. Cerreta, J. Bingert
Los Alamos
Operated by Los Alamos National Security, LLC for NNSA
NNSA

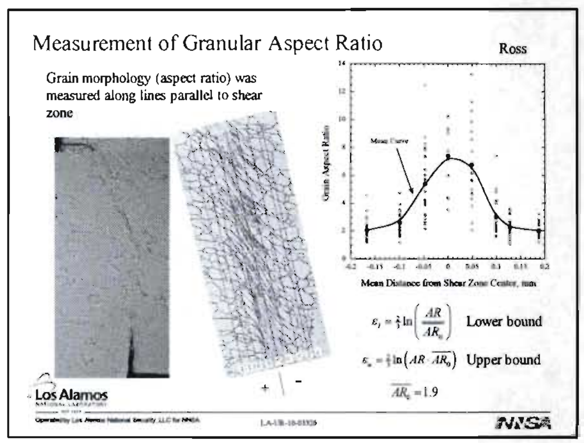
Measurement of Granular Aspect Ratio
Ross
Grain morphology (aspect ratio) was measured along lines parallel to shear zone
Mean Distance from Shear Zone Center, mm
Lower bound
Upper bound
Los Alamos
Operated by Los Alamos National Security, LLC for NNSA
NNSA

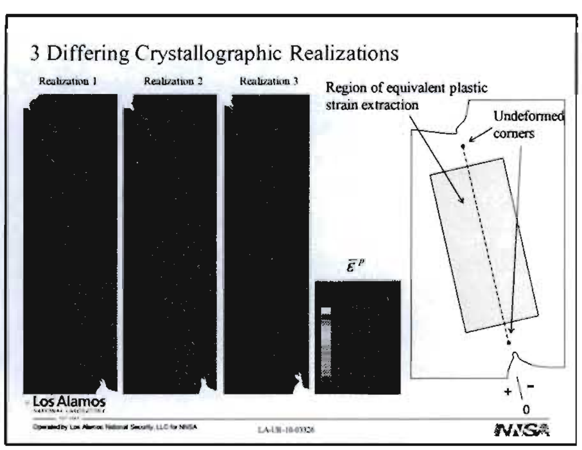
3 Differing Crystallographic Realizations
Realization 1
Realization 2
Realization 3
Region of equivalent plastic strain extraction
Undeformed corners
Los Alamos
Operated by Los Alamos National Security, LLC for NNSA
NNSA

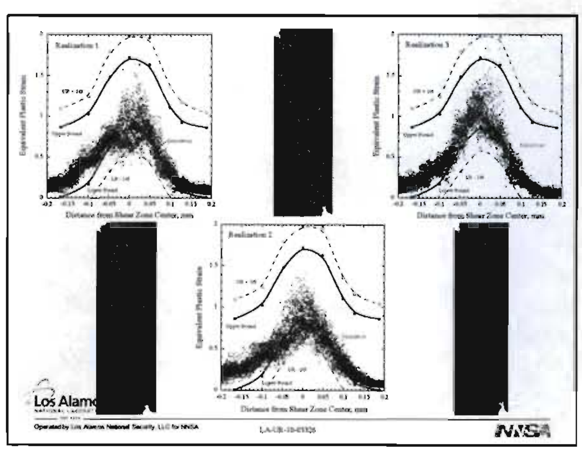
Realization 1
Realization 3
Realization 2
Distance from Shear Zone Center, mm
Operated by Los Alamos National Security, LLC for NNSA
NNSA

Shear zone region interrogation by nano-indentation

- Hysitron triboindenter – Berkovich pyramidal tip
- 10 measurement zone width – 4 micron step
- Penetration depth – 200 nm
- Loading/unloading rate – 10 nm/s
- Hold time – 10 s

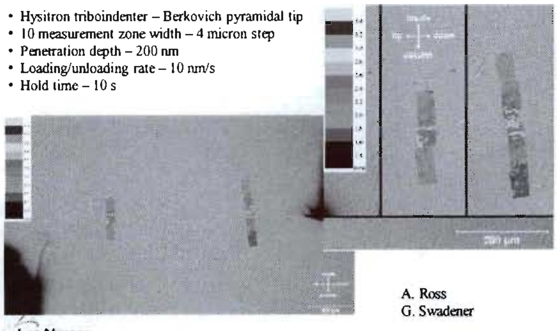

A. Ross
G. Swadener

Shear zone interrogation by nano-indentation

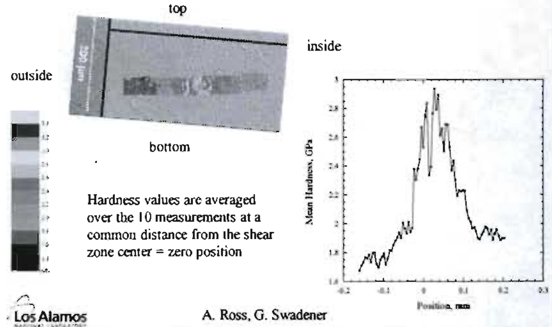

A. Ross, G. Swadener

Summary & comments

- Damage and failure in polycrystalline metallic materials is strongly dependent upon microstructural details – modern lower length scale tools are necessary to assist in our learning about these complex physical processes. This can then properly motivate the development of physically based higher length scale models for use in applications.
- In general, we do not have the ability to adequately represent the topology of polycrystalline microstructures – this is especially true in 3D. Sub-granular initial state is also a concern.
- The modeling results compare OK with experimental measurements. Comments are:
  - Stress response is consistently over-predicted.
  - Texture prediction clearly shows 2D deformation gradient.
  - Shear zone strain profile is well predicted.
  - Due to tessellation limitations, triangular elements were required.

Tophat Experiments

Results from tophat experiments performed at 25 C

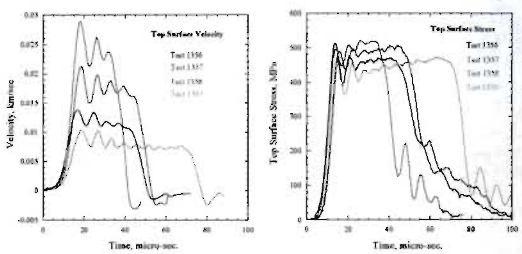

Localization - Ta

- Dynamic response of the SHPB system is not represented
- Piecewise linear velocity profile applied uniformly to the top surface
- Top surface stress response is weighted average of top row of elements

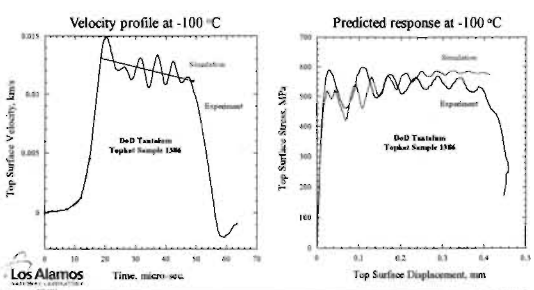

Localization

- FE code EPIC - explicit
- Axisymmetric and adiabatic
- 46,000 triangular elements
- 2000 shear section elements
- Contact friction surfaces in two corners
- Velocity profile applied to top surface
- Rigid and frictionless base
- Stress response at top surface compared to experiments

Low density mesh shown

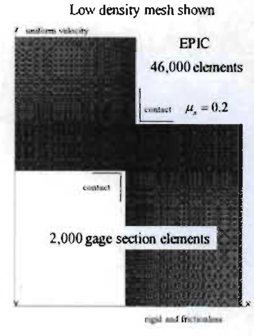

Continuum Model

Addessio and Johnson, 1993; Maudlin et al., 1999
Mason, 1999, 2004

Stress

$$\mathbf{T} = \mathbf{M}\tilde{\mathbf{T}} \qquad \underline{\mathbf{M}} = (1-\phi)\underline{\mathbf{I}}$$

$$\dot{\tilde{\mathbf{T}}} = \underline{\mathbf{M}}\underline{\mathbf{L}}^{-1}\left(\mathbf{D}' - \mathbf{D}^{p'}\right) - \underline{\mathbf{M}}\left(-\frac{\partial \tilde{P}}{\partial \beta}\mathrm{tr}\mathbf{D}^{e} + \frac{\tilde{\rho}}{\rho}\Gamma \mathbf{T}\cdot\mathbf{D}^{p}\right)\underline{\mathbf{I}} + \dot{\underline{\mathbf{M}}}\underline{\mathbf{M}}^{-1}\mathbf{T}$$

Strain Rate

$$\mathbf{D} = \mathbf{D}^{e} + \mathbf{D}^{p} = \mathbf{D}^{e} + \mathbf{D}^{d} + \mathbf{D}^{p'}$$

Plastic Flow Rate

$$\mathbf{D}^{p} = \frac{1}{\tau_r}\left(\mathbf{T} - \mathbf{T}^{proj}\right)$$

$\tau_r = 70$ Pa·s
$q_1 = 1.5$
$q_2 = 0.625$
$q_3 = 2.25$

$$\tau - \sigma_f(\dot{\varepsilon},\theta)^2\left[1 + q_3\phi^2 - 2q_1\phi\cosh\delta\right] = 0$$

$$\tau = \frac{1}{2}\mathbf{T}'\cdot\underline{\alpha}\cdot\mathbf{T}' \qquad \delta = -\frac{3q_2\tilde{P}}{2\sigma_s} \qquad \tilde{P} = -\tfrac{1}{3}\mathrm{tr}\tilde{\mathbf{T}}$$

Damage Rate $\mathrm{tr}\mathbf{D}^{p} > 0$

$$\mathbf{D}^{d} = \frac{\dot{\phi}}{3(1-\phi)}\underline{\mathbf{I}} \qquad \dot{\phi} = (1-\phi)\mathrm{tr}\mathbf{D}^{p}$$

$\phi_0 = 0.0003$

Equation of State

$$\tilde{P} = \left(K_1\tilde{\beta} + K_2\tilde{\beta}^2 + K_3\tilde{\beta}^3\right)\left(1 - \Gamma\tilde{\beta}/2\right) + \Gamma\tilde{E}_s\left(1+\tilde{\beta}\right)$$

$$\tilde{\beta} = \frac{\tilde{\rho}}{\tilde{\rho}_0} - 1 \qquad \rho = (1-\phi)\tilde{\rho}$$

$K_1 = 196.8$ GPa $\quad \Gamma = 1.60$
$K_2 = 259.8$ GPa $\quad \rho_0 = 16{,}640$ kg/m^3
$K_3 = 256.6$ GPa

Plastic Work

$$\dot{\theta} = \frac{\eta}{\rho C_v}\dot{E}_s$$

$\eta = 0.95$
$C_v = 54.4$ J/kg·K

Localization - Ta

- Predicted responses for sample 1356 and 1357 experiments performed at 25 °C

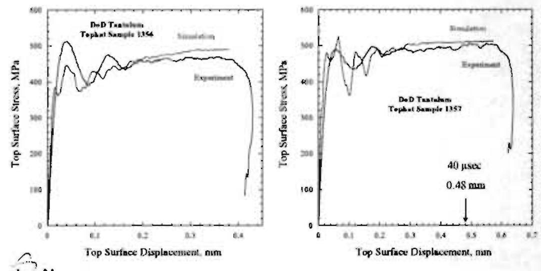

Continuum Model – Sample 1357
Time = 40 micro-sec.

- Contact friction significant in top corner
- Damage plays no role
- Shear band does not form

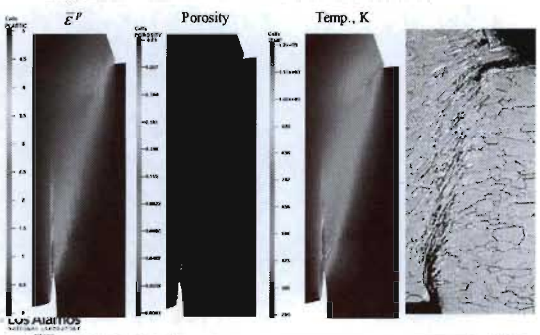

Shear Band – 316 SS

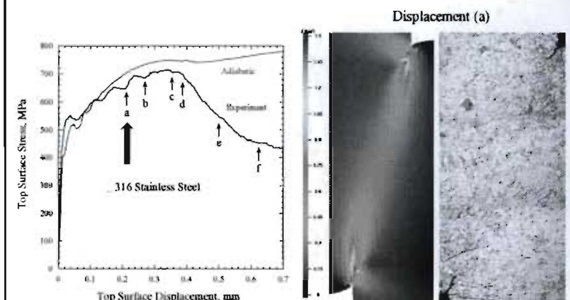

Shear Band – 316 SS

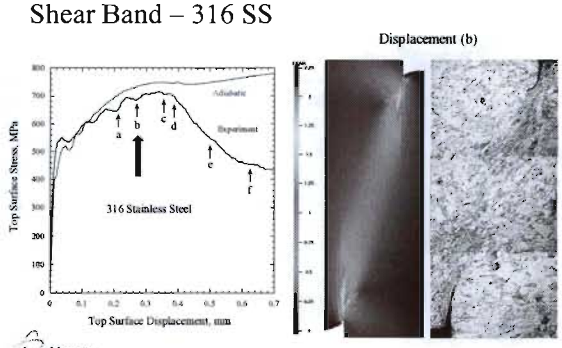

Shear Band – 316 SS

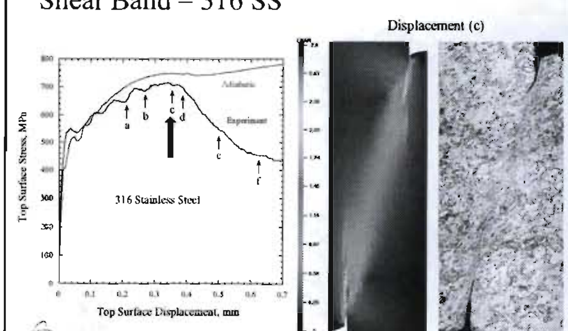

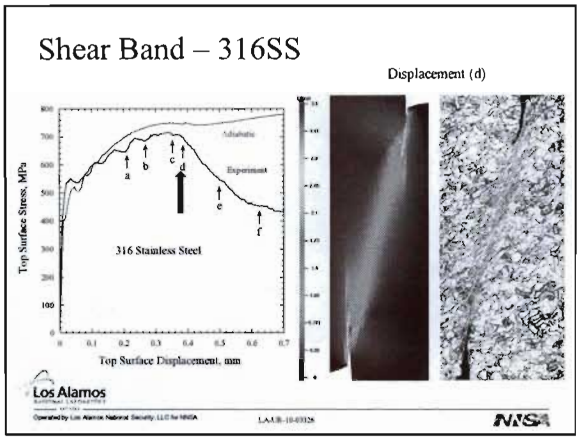
Shear Band – 316SS
Displacement (d)
Adiabatic
Experiment
316 Stainless Steel
Top Surface Stress, MPa
Top Surface Displacement, mm
Los Alamos
NNSA

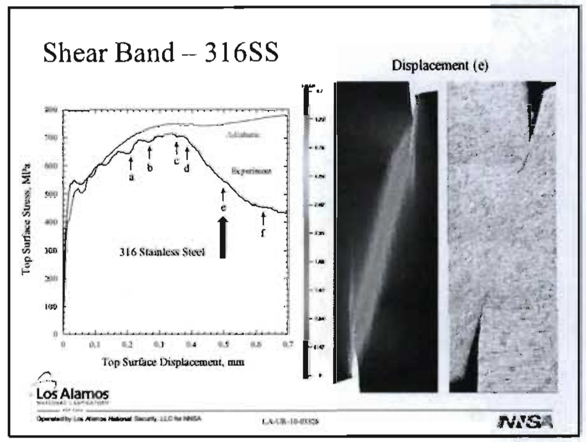
Shear Band – 316SS
Displacement (e)
Adiabatic
Experiment
316 Stainless Steel
Top Surface Stress, MPa
Top Surface Displacement, mm
Los Alamos
NNSA

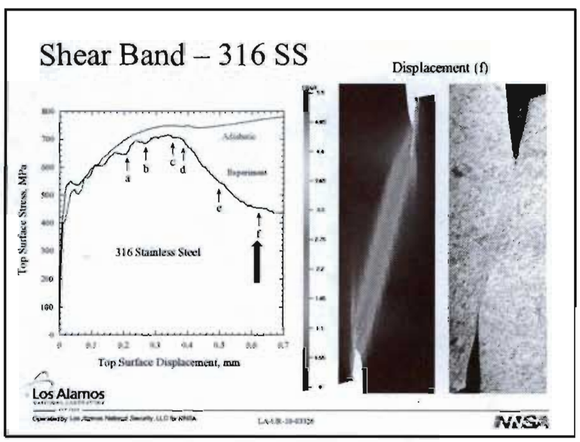
Shear Band – 316 SS
Displacement (f)
Adiabatic
Experiment
316 Stainless Steel
Top Surface Stress, MPa
Top Surface Displacement, mm
Los Alamos
NNSA

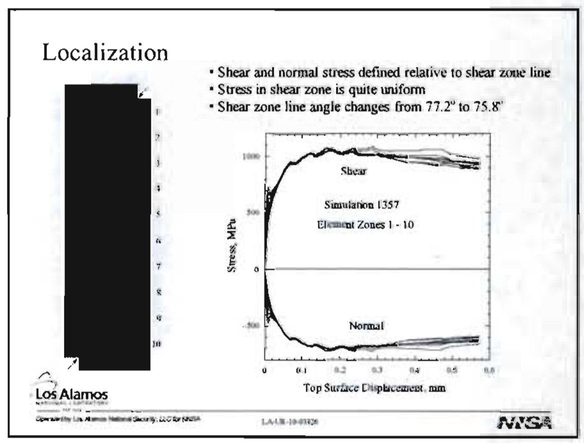
Localization
• Shear and normal stress defined relative to shear zone line
• Stress in shear zone is quite uniform
• Shear zone line angle changes from 77.2° to 75.8°
Shear
Simulation 1357
Element Zones 1 - 10
Normal
Stress, MPa
Top Surface Displacement, mm
Los Alamos
NNSA

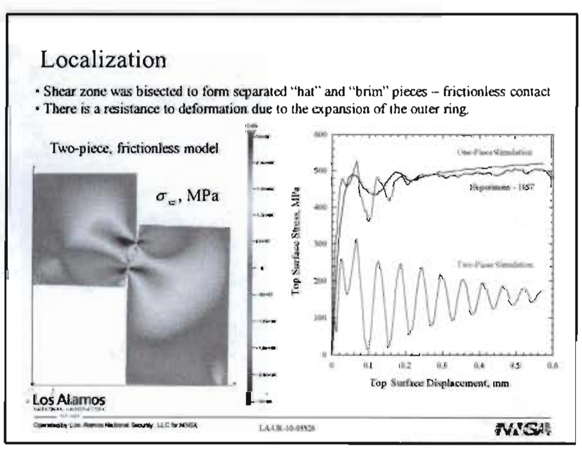
Localization
• Shear zone was bisected to form separated "hat" and "brim" pieces – frictionless contact
• There is a resistance to deformation due to the expansion of the outer ring.
Two-piece, frictionless model
σ, MPa
One-Piece Simulation
Experiment - 1357
Two-Piece Simulation
Top Surface Stress, MPa
Top Surface Displacement, mm
Los Alamos
NNSA

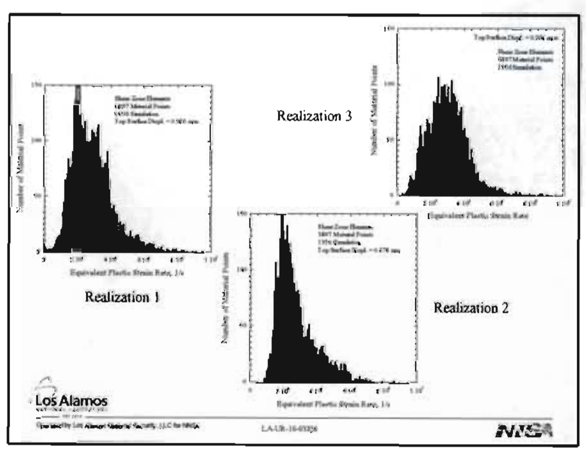
Realization 3
Realization 1
Realization 2
Number of Material Points
Equivalent Plastic Strain Rate, 1/s
Los Alamos
NNSA

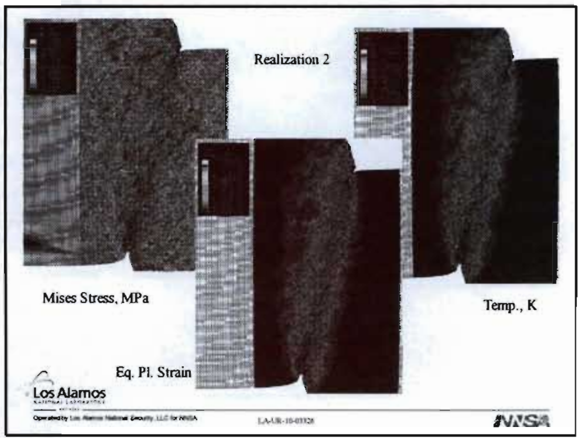
Realization 2
Mises Stress, MPa
Temp., K
Eq. Pl. Strain
Los Alamos
NNSA

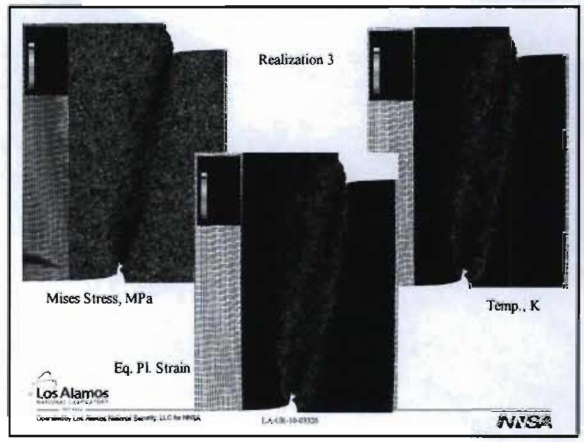
Realization 3
Mises Stress, MPa
Temp., K
Eq. Pl. Strain
Los Alamos
NNSA

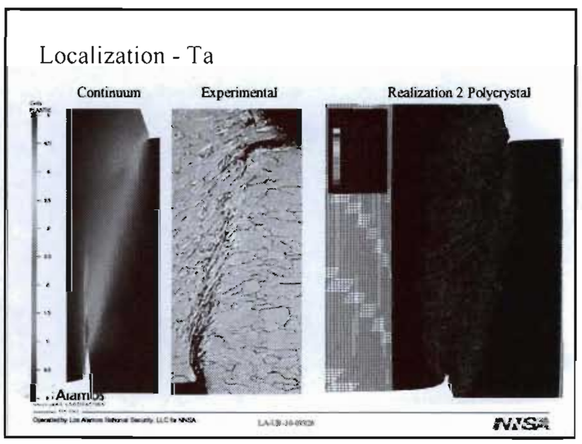
Localization - Ta
Continuum
Experimental
Realization 2 Polycrystal
NNSA

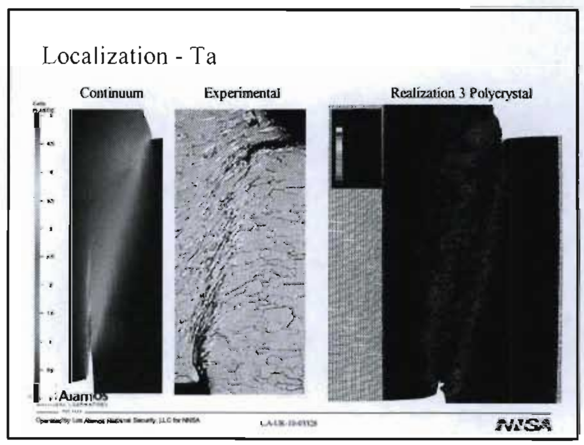
Localization - Ta
Continuum
Experimental
Realization 3 Polycrystal
NNSA

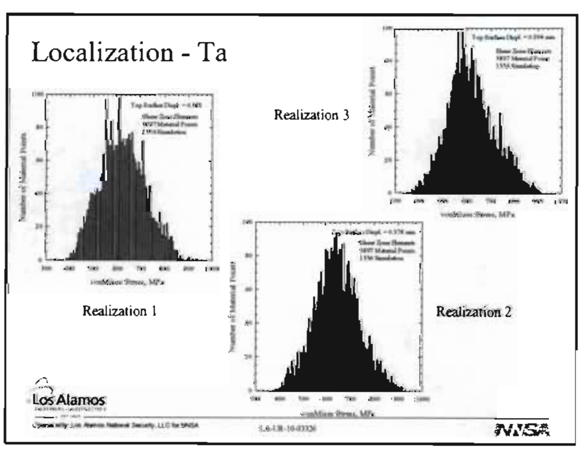
Localization - Ta
Realization 3
Realization 1
Realization 2
Los Alamos
NNSA

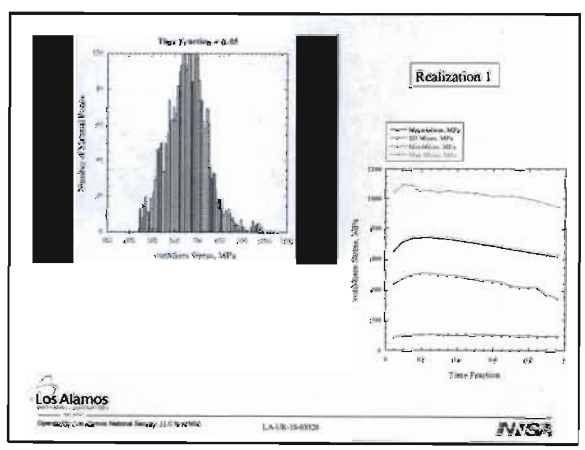
Realization 1
Los Alamos
NNSA

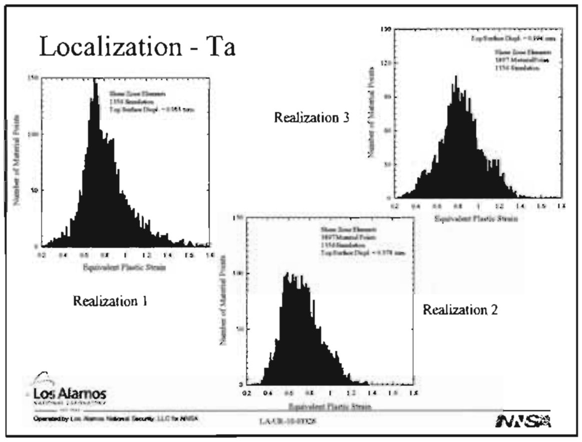
Localization - Ta
Realization 3
Realization 1
Realization 2
Los Alamos

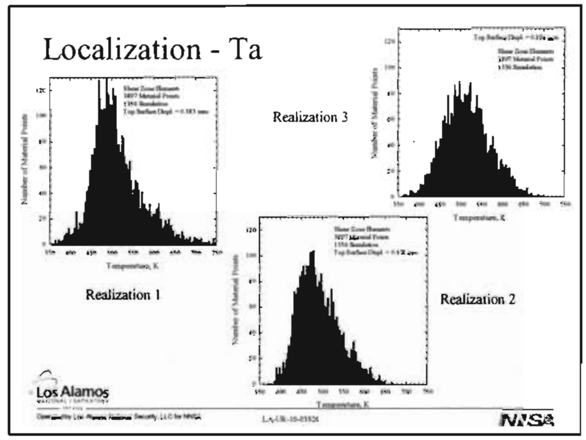
Localization - Ta
Realization 3
Realization 1
Realization 2
Los Alamos

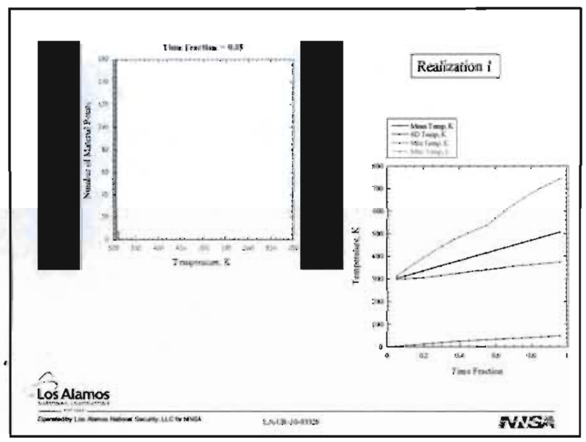
Realization 1
Los Alamos

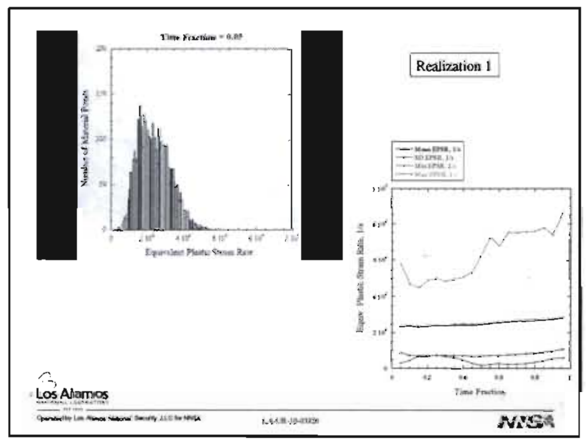
Realization 1
Los Alamos

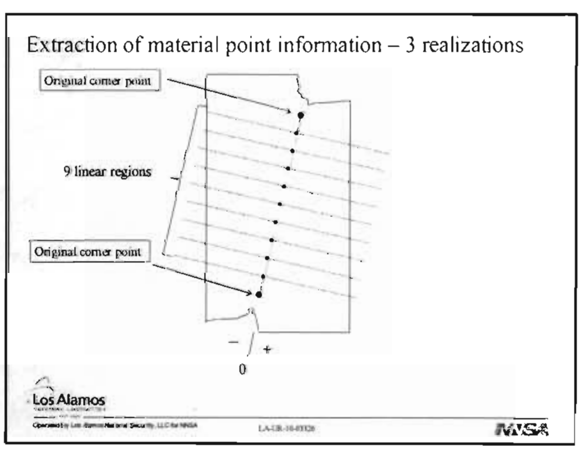
Extraction of material point information – 3 realizations
Original corner point
9 linear regions
Original corner point
0
Los Alamos

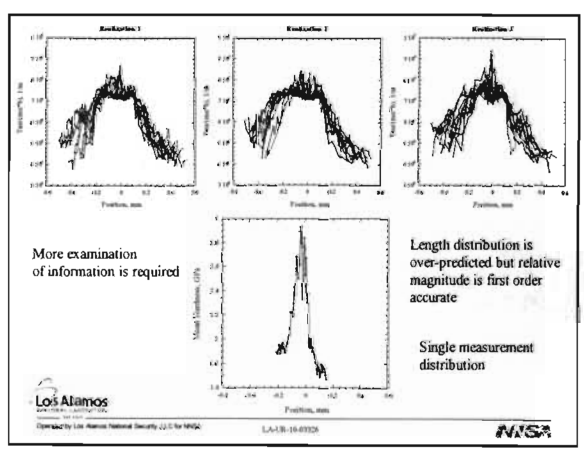
More examination
of information is required
Length distribution is
over-predicted but relative
magnitude is first order
accurate
Single measurement
distribution
Los Alamos

Extraction of material point information – 3 realizations

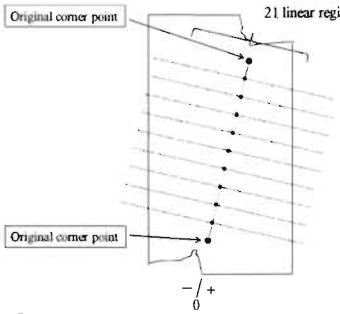

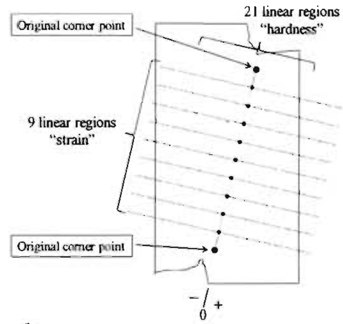

Extraction of material point information – 3 realizations

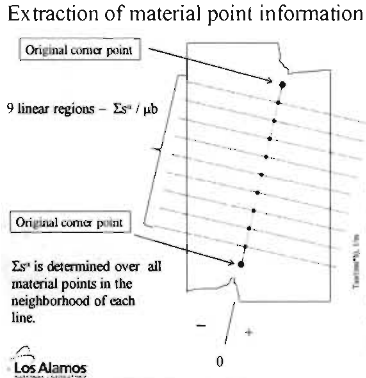

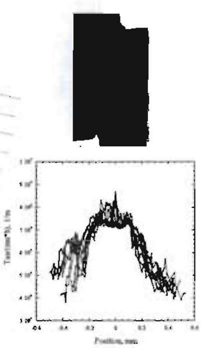

Stochastic Mean-field Polycrystal Plasticity Methods

Dissertation Defense

Michael Tonks

Department of Mechanical Science and Engineering
University of Illinois at Urbana-Champaign

July 2, 2008

Acknowledgements

- Daniel A. Tortorelli and Armand J. Beaudoin
  - *University of Illinois at Urbana-Champaign*
- Eric Harstad, John Bingert, Paul Maudlin, Curt Bronkhorst, Frank Addessio, and Ben Hansen
  - *Los Alamos National Laboratory*
- Frank Schilder
  - *University of Surrey*
- Center for Simulation of Advanced Rockets at the University of Illinois at Urbana-Champaign
- Joint Department of Energy and Department of Defense Munitions Technology Development

Polycrystal Plasticity

- Crystal structure influences macro-scale deformation

Raabe and Roters, 2004

Polycrystal Plasticity

- Single crystal plasticity
  - Occurs primarily by shearing along slip planes
  - Crystal rotates as it deforms
- Polycrystal plasticity
  - Crystals rotate towards preferred orientations determined by the crystal structure and loading

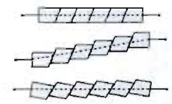

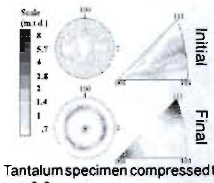

Tantalum specimen compressed to $\varepsilon = -2.0$

Single Crystal Model

Dislocation generation and pile-up accounted for by increasing slip resistance with a hardening law

Crystal reorientation obtained from kinematics

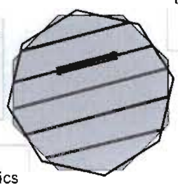

Plastic deformation due to slip along slip planes

$$L_p^c = \sum_{s=1}^{M} \dot{\gamma}^s \, b_0^s \otimes n_0^s$$

Dislocation motion defined by a flow rule

$$\dot{\gamma}^s = \hat{\dot{\gamma}}^s(\tau^s, \tau_0^s)$$

Crystal Plasticity Finite Element Method (CPFEM)

- Models a polycrystal aggregate of *N* crystals
- Each crystal represented by one or more elements
- Advantages:
  - Explicitly models crystal interactions
  - Includes topology
- Disadvantages:
  - Too expensive for large numbers of crystals

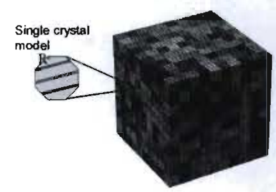

Mean-Field Polycrystal Plasticity Models

- Also models a polycrystal aggregate of *N* crystals

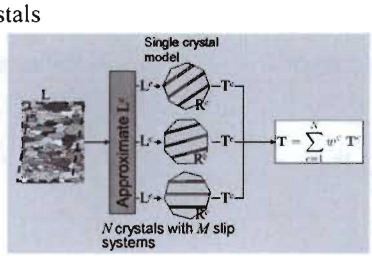

Fully Constrained Model (FCM)

- Crystals follow Taylor hypothesis: $\mathbf{L}^c = \mathbf{L}$
- Upper-bound model, ensures compatibility

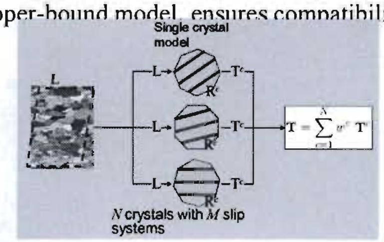

Taylor (1938)

No-Constraints Model (NCM)

- Homogeneous stress state: $\mathbf{T}^c = \mathbf{T}$
- Lower-bound model, ensures stress equi

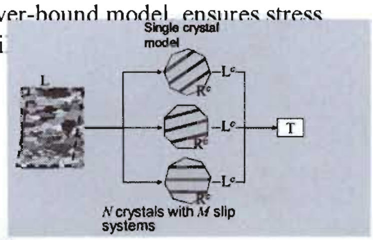

Los Alamos

Chastel and Dawson (1994)

NNSA

Multi-Grain Relaxed Constraint Models (RCM)

- Ave($\mathbf{L}^c$) = $\mathbf{L}$ for compatible groups of 2 or 8 crystals
-

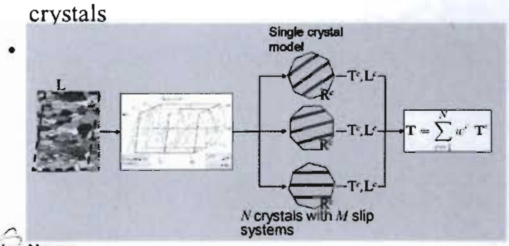

Los Alamos

Van Houtte et al. (1999), Crumbach et al. (2001)

NNSA

Visco-Plastic Self-Consistent (VPSC) Model

- Treats each grain as an ellipsoidal inclusion in an average homogeneous effective medium (

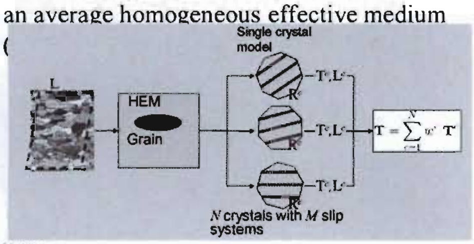

Los Alamos

Lebensohn and Tomé (1993)

NNSA

Modeling Macro-scale Polycrystalline Bodies

- Micro-structure driven yield surface
  - Mean-field aggregate model used to generate a yield surface for a macro-scale phenomenologic plasticity analysis

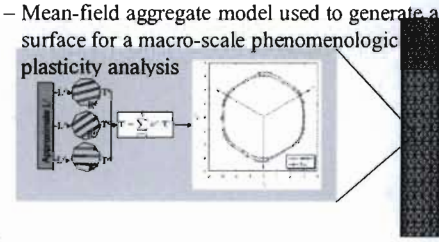

Los Alamos

Shaffer and Maudlin (1998), Van Houtte et al. (1995), Maudlin et al. (2003)

NNSA

Modeling Macro-scale Polycrystalline Bodies

- Embedded mean-field aggregate model
  - Mean-field aggregate model used at each material point to predict the material behavior

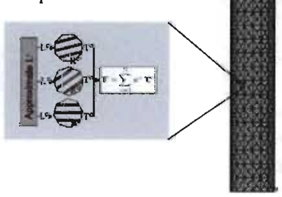

Los Alamos

NNSA

Improving L^c Approximation Methods

- Accuracy of mean-field model depends on the method used to approximate $\mathbf{L}^c$
- $\mathbf{L}^c$ can not be easily obtained experimentally
- An idealization can be garnered with the CPFEM

Los Alamos

NNSA

Stochastic Method Motivation

- CPFEM analysis by Sarma and Dawson (1996)
  - …rmal distribution with

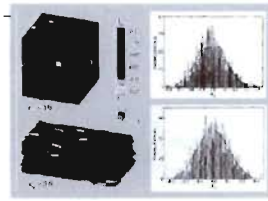

- Plain strain compression
- copper cubic aggregate
- 1000 crystals
- 1 element/crystal
- Random and simulated initial textures

Los Alamos

~~Sarma and Dawson (1996)~~

NNSA

Stochastic Methods

- Treat $\mathbf{D}^c$ as a normally distributed random tensor
- I…
  …

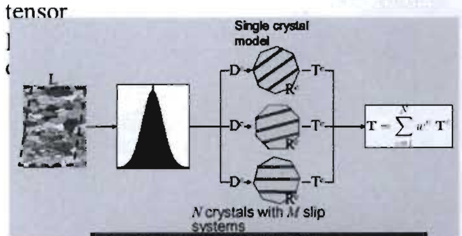

- Based on limited CPFEM data
- Not based on micro-mechanical principles

Los Alamos

~~Engler (2002); Marc et al. (2004)~~

NNSA

Presentation Summary

- Purpose: To establish the validity of stochastic models for approximating $\mathbf{L}^c$ and to develop two such models.
- Outline
  - Planar polycrystal
  - 3-D CPFEM analysis
  - 3-D Stochastic method formulation, calibration, and validation
  - Tantalum Taylor impact specimen analysis
- Conclusions and future work

Los Alamos

NNSA

CPFEM ABAQUS UMAT

Asaro & Rice (1977), Acharya & Beaudoin (2000), Kothari & Anand (1998), Busso et al. (2000), Kocks (1976) Kalidindi et al. (1992), Bronkhorst et al. (1992), Anand (1998)

- Single crystal model

Stress

$$\mathbf{T}^{c*} = \mathcal{C}(\theta^c)\,[\mathbf{E}^c_e - \mathbf{A}(\theta^c - \theta_0)]$$
$$\mathcal{C}(\theta^c) = \mathcal{C}_0 + \mathcal{M}(\theta^c)$$
$$\mathbf{F}^c = \mathbf{F}^c_e \mathbf{F}^c_p$$
$$\mathbf{E}^c_e = \frac{1}{2}\left(\mathbf{F}^{cT}_e \mathbf{F}^c_e - \mathbf{I}\right)$$

Flow Rule

$$\mathbf{L}^c_p = \dot{\mathbf{F}}^c_p \mathbf{F}^{c-1}_p = \sum_{\alpha=1}^{M} \dot{\gamma}^\alpha\, \mathbf{b}^\alpha_0 \otimes \mathbf{n}^\alpha_0$$
$$\dot{\gamma}^\alpha = \dot{\gamma}^\alpha(\tau^\alpha) = \dot{\gamma}_0 \exp\left[-\frac{F_0}{k\theta^c}\left\langle 1 - \left\langle \frac{|\tau^\alpha| - \tau^\alpha_0 \frac{\mu}{\mu_0}}{\hat{\tau}\frac{\mu}{\mu_0}} \right\rangle^p \right\rangle^q\right] \mathrm{sign}(\tau^\alpha)$$
$$\frac{\mu}{\mu_0} = 1 + \frac{\mathcal{M}_{1212}}{\mathcal{C}_{1212_0}}\theta^c$$
$$\tau^\alpha = (\mathbf{R}^c \mathbf{m}^\alpha_0\, \mathbf{R}^{cT}) \cdot \mathbf{T}^{c\prime}$$

Hardening

$$\dot{\tau}^\alpha_0 = \sum_\beta h_{\alpha\beta}\,|\dot{\gamma}^\beta|$$
$$h_{\alpha\beta} = [r + (1 - r)\delta_{\alpha\beta}]\, h_\beta$$
$$h_\beta = h_0\left(\frac{s^\beta_s - \tau^\beta_0}{s^\beta_s - \tau_{0_0}}\right), \quad s^\beta_s = s^\beta_s(\dot{\gamma}^\beta, \theta^c) = s_{s_0}\left(\frac{\dot{\gamma}^\beta}{\dot{\gamma}_{s_0}}\right)^{\frac{k\theta^c}{A}}$$

Adiabatic Heating

$$\dot{\theta}^c = \frac{\eta}{\rho c_p}\sum_{\alpha=1}^{N} \tau^\alpha \dot{\gamma}^\alpha$$

Los Alamos

~~Bronkhorst et al. (2007)~~

NNSA

CPFEM Model

- Material parameters from Bronkhorst *et al.*

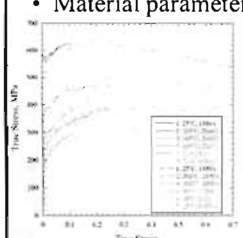

Parameter	Value	Units	Parameter	Value	Units
$\mathcal{C}_{1111_0}$	268.5	GPa	$\mathcal{M}_{1111}$	-0.0245	GPa/K
$\mathcal{C}_{1122_0}$	159.8	GPa	$\mathcal{M}_{1122}$	-0.0118	GPa/K
$\mathcal{C}_{1212_0}$	87.1	GPa	$\mathcal{M}_{1212}$	-0.0129	GPa/K
$\dot{\gamma}_0$	10^7	sec^{-1}	F_0	2.1×10^{-19}	J
$\hat{\tau}$	0.55	GPa	[illegible]	0.05	GPa
p	0.34		η	1.66	
q	1.4		h_0	0.3	GPa
A	[illegible]	J	[illegible]	0.125	GPa
ρ	16640	kg/m^3	c_p	150	J/kg-K
η	0.95		θ_0	298	K
α	6.5	$\mu m/m$-K			

Los Alamos

Operated by Los Alamos National Security, LLC for NNSA

NNSA

I. Preferred Orientations in Planar Polycrystals

Los Alamos

Operated by Los Alamos National Security, LLC for NNSA

NNSA

Texture Evolution

- FCM analyses show textures either evolve towards preferred orientations or oscillate
  - Depends on the magnitude of the applied spin.
  - True ... an ... stals

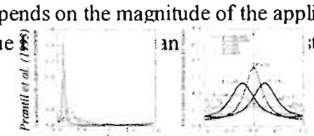

- Purpose: Investigate texture evolution in planar polycrystal with 2 slip systems using stochastic Taylor model (STM) and CPFEM

Los Alamos

Prantil et al. (1993), Kumar and Dawson (1996), Kumar (1996)

NNSA

Single Crystal Kinematics

- $\mathbf{F}^c = \mathbf{R}^c \mathbf{F}_p^c$
- $\mathbf{L}^c = \dot{\mathbf{F}}^c \mathbf{F}^{c\,-1} = \dot{\mathbf{R}}^c \mathbf{R}^{c\,T} + \mathbf{R}^c \mathbf{L}_p^c \mathbf{R}^{c\,T}$

  $\mathbf{L}_p^c = \dot{\mathbf{F}}_p^c \mathbf{F}_p^{c-1} = \sum_{s=1}^{M} \dot{\gamma}^s \mathbf{b}_0^s \otimes \mathbf{n}_0^s$

  $\mathbf{D}^c = \mathbf{R}^c \mathbf{D}_p^c \mathbf{R}^{c\,T}$
- $\mathbf{W}^c = \dot{\mathbf{R}}^c \mathbf{R}^{c\,T} + \mathbf{R}^c \mathbf{W}_p^c \mathbf{R}^{c\,T}$
- Orientation evolution

  $\dot{\mathbf{R}}^c = \mathbf{W}^c \mathbf{R}^c - \mathbf{R}^c \mathbf{W}_p^c$

Los Alamos

LA-UR-10-03326

NNSA

Orientation Change for a Crystal c

- $\mathbf{R}^c(\theta^c) = \begin{bmatrix} \cos\theta^c & -\sin\theta^c \\ \sin\theta^c & \cos\theta^c \end{bmatrix}$ $\mathbf{L}^c = \begin{bmatrix} \Gamma^c & \Lambda^c + \Omega^c \\ \Lambda^c - \Omega^c & -\Gamma^c \end{bmatrix}$
- $\dot{\gamma}^1 = 2\csc 4\beta\,(\Gamma^c \sin 2(\beta - \theta^c) - \Lambda^c \cos 2(\beta - \theta^c))$

  $\dot{\gamma}^2 = 2\csc 4\beta\,(\Gamma^c \sin 2(\beta + \theta^c) + \Lambda^c \cos 2(\beta + \theta^c))$

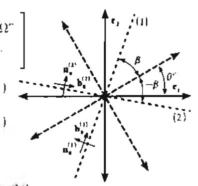

- Crystal reorientation equation

  $\dot{\theta}^c = -\Omega^c + \lambda(\Gamma^c \cos 2\theta^c - \Lambda^c \sin 2\theta^c) \quad \lambda \equiv \sec 2\beta$
- Texture at time t

  $\theta^c = \tan^{-1}\left[\frac{(-\lambda\Lambda^c + \mathcal{F}\tanh[t\mathcal{F} + \tanh^{-1}[\frac{1}{\mathcal{F}}(\lambda\Lambda^c + (\lambda\Gamma^c + \Omega^c)\tan\theta_0^c)]])}{(\Gamma^c\lambda + \Omega^c)^{-1}}\right]$

  $\mathcal{F} = \sqrt{\lambda^2(\Gamma^{c\,2} + \Lambda^{c\,2}) - \Omega^{c\,2}}$

Los Alamos

LA-UR-10-03326

NNSA

The Kuramoto Model

- Models the phase change of coupled oscillators
  - Sinusoidal coupling: $\dot{\theta}_i = \omega_i - Kr\sin\theta_i$
  - If $Kr \geq |\omega_i|$ system approaches stable point
  - If $Kr < |\omega_i|$ system drifts
- Similar to planar polycrystal texture evolution
  - $\dot{\theta}^c = -\Omega^c + \lambda(\Gamma^c \cos 2\theta^c - \Lambda^c \sin 2\theta^c)$

Complex Order Parameter

$re^{i\psi} = \frac{1}{N}\sum_{j=1}^{N} e^{i\theta_j}$

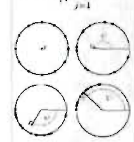

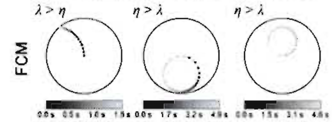

$\Omega = -1.3, \Gamma = 1,$ and $\Lambda = 0$ $\quad$ $\Omega = 2.1, \Gamma = 0,$ and $\Lambda = 1$ $\quad$ $\Omega = -\pi, \Gamma = 0,$ and $\Lambda = 1.2$

$\lambda \equiv \sec 2\beta$

$\eta = \frac{|\Omega^c|}{\sqrt{\Gamma^{c2} + \Lambda^{c2}}} = \frac{|\Omega|}{\sqrt{\Gamma^2 + \Lambda^2}}$

Los Alamos

LA-UR-10-03326

NNSA

CPFEM Analysis of the Planar Polycrystal

- Planar polycrystal with $N = 900$ crystals

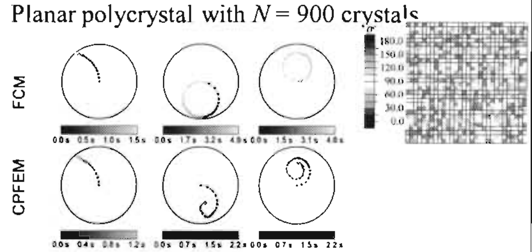

$\Omega = -1.3, \Gamma = 1,$ and $\Lambda = 0$ $\quad$ $\Omega = 2.1, \Gamma = 0,$ and $\Lambda = 1$ $\quad$ $\Omega = -\pi, \Gamma = 0,$ and $\Lambda = 1.2$

Los Alamos

LA-UR-10-03326

NNSA

Crystal Orientation Spatial Distribution

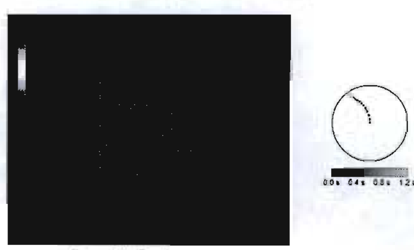

$\Omega = -1.3, \Gamma = 1,$ and $\Lambda = 0$

Los Alamos

LA-UR-10-03326

NNSA

Crystal Orientation Spatial Distribution

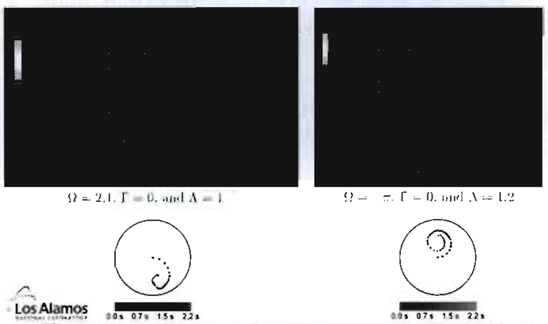

Statistical Behavior of L^c

- Distribution of L^c

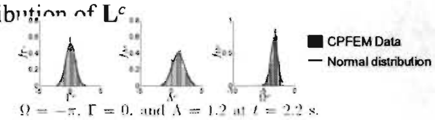

- Standard deviations over time

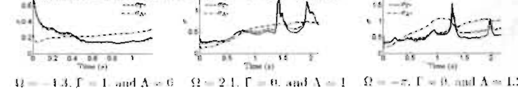

Planar STM Formulation

- Treat $\mathbf{D}^c$ as normally distributed random tensor

Stochastic Taylor Model (STM)

- $f_{\Gamma^c}(x) = \frac{e^{-\frac{(-\Gamma+x)^2}{2\sigma^2}}}{\sqrt{2\pi}\sigma}$, $f_{\Lambda^c}(y) = \frac{e^{-\frac{(-\Lambda+y)^2}{2\sigma^2}}}{\sqrt{2\pi}\sigma}$, $\Omega^c(t) = \Omega$, $\eta^c = \frac{|\Omega|}{\sqrt{\Gamma^{c\,2} + \Lambda^{c\,2}}}$

$P(\lambda > \eta^c)$ Assume σ is constant

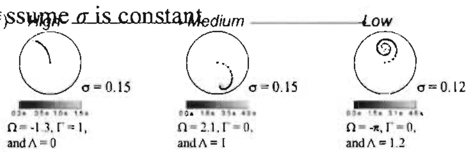

Texture Evolution Comparison

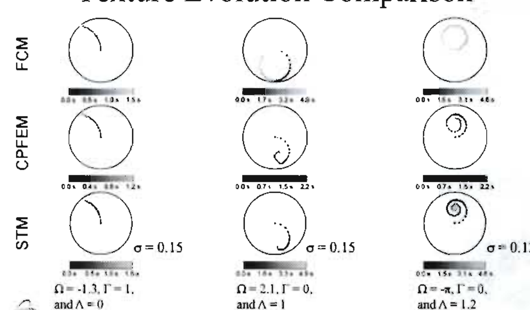

Effect of Standard Deviation

$P(\lambda > \eta^c)$

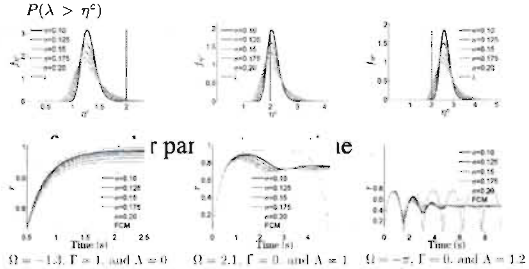

Planar Polycrystal Analysis Conclusions

- There is a link between polycrystal texture evolution and the synchronization of coupled oscillators
- The STM and the CPFEM predict that the texture converges to a steady-state distribution
- The STM is more accurate than the FCM and nearly as simple

II. 3-D CPFEM analysis

CPFEM Analysis Summary

- Tantalum polycrystal with 1000 cubic g
  - 24 slip systems: {110} <111> and {112} <

$$L_1 = \begin{bmatrix} 500 & 0 & 250 \\ 0 & 500 & 0 \\ -250 & 0 & -1000 \end{bmatrix}\frac{1}{s},\ L_2 = \begin{bmatrix} 1000 & 200 & 0 \\ -200 & 0 & 0 \\ 0 & 0 & -1000 \end{bmatrix}\frac{1}{s},\ L_3 = \begin{bmatrix} 0 & 0 & 1000 \\ 0 & 0 & 0 \\ 0 & 0 & 0 \end{bmatrix}\frac{1}{s}$$

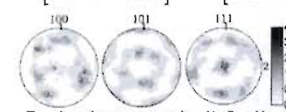

- Two initial textures
  - Random texture

Tantalum plate texture analyzed in Bronkhorst et al. 2007

Convergence Study

- Investigate sen... to number elements per cr...
- Deform polycry... with random initial texture a... gradient L_1 for

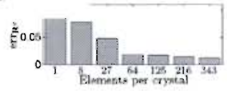

PDFs of D^c and W^c

- Approximately follow normal distributions
  - $\mu_{D^c} = D$ and $\mu_{W^c} = W$

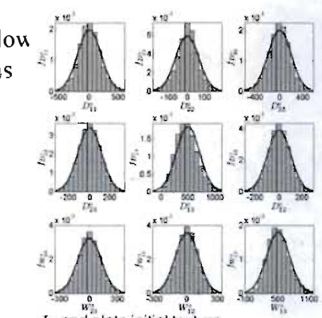

L_2 and plate initial texture

Reason for Normal Distribution

- The L^c experienced by an element in a CPFEM analysis is determined by the
  - Crystal orientation
  - Material parameters
  - Applied boundary conditions
  - Interactions between neighboring crystals/elements
- Distribution shape is due to the crystal interactions

Covariance Tensors

- Normal distributions are defined by 2nd-order tensors and order covariance tensors
  - $\mu_{D^c} = D$ and $\mu_{W^c} = W$
- Calculated according to
  - $\Sigma_{D^c} = \frac{1}{N}\sum_{c=1}^{N}(D^c - \mu_{D^c}) \otimes (D^c - \mu_{D^c})$
  - $\Sigma_{W^c} = \frac{1}{N}\sum_{c=1}^{N}(W^c - \mu_{W^c}) \otimes (W^c - \mu_{W^c})$
- We determine the six eigenvalues σ_i^2 of Σ_{D^c} and the three eigenvalues γ_i^2 of Σ_{W^c}

Eigenvalues of Covariance Tensors

- $\mathbf{L}_1$

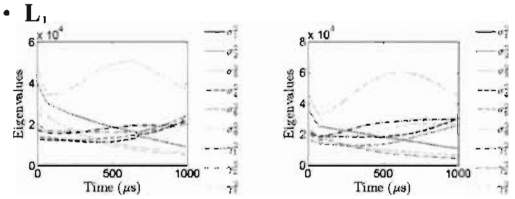

Random initial texture

Plate initial texture

$$\mathbf{L}_1 = \begin{bmatrix} 500 & 0 & 200 \\ 0 & 500 & 0 \\ -200 & 0 & -1000 \end{bmatrix} \frac{1}{s}$$

Los Alamos

NNSA

Eigenvalues of Covariance Tensors

- $\mathbf{L}_2$

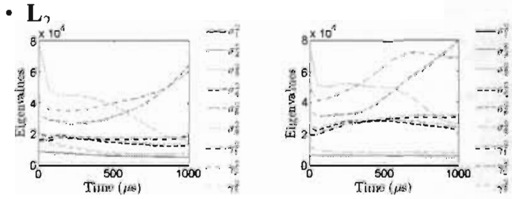

Random initial texture

Plate initial texture

$$\mathbf{L}_2 = \begin{bmatrix} 1000 & 200 & 0 \\ -200 & 0 & 0 \\ 0 & 0 & -1000 \end{bmatrix} \frac{1}{s}$$

Los Alamos

NNSA

Eigenvalues of Covariance Tensors

- $\mathbf{L}_3$

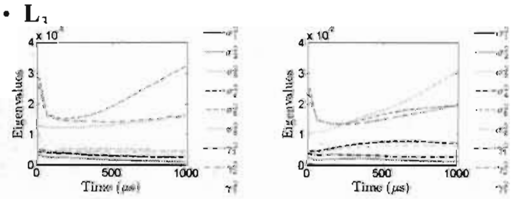

Random initial texture

Plate initial texture

$$\mathbf{L}_3 = \begin{bmatrix} 0 & 0 & 1000 \\ 0 & 0 & 0 \\ 0 & 0 & 0 \end{bmatrix} \frac{1}{s}$$

Los Alamos

NNSA

D^c Covariance Tensor

- Has one zero eigenvalue,
  - $\Phi_1 \approx \frac{1}{\sqrt{3}}\mathbf{I}$ficient $\mathrm{tr}(\mathbf{D}^c) \approx \mathrm{tr}(\mathbf{D})$ng eigentensor $\Phi_1 \approx 1/3\ \mathbf{I}$
-
  - Crystal interactions dominated by isochoric plastic strain
  - Crystals experience the volumetric deformation

$$\mathbf{L}_2 = \begin{bmatrix} 1000 & 200 & 0 \\ -200 & 0 & 0 \\ 0 & 0 & -1000 \end{bmatrix} \frac{1}{s}$$ Plate initial texture

$$\mu_{\mathrm{tr}(\mathbf{D}^c)} - \mathrm{tr}(\mathbf{D}_2) = -4.1 \times 10^{-3} \|\mathbf{D}_2\|$$
$$\sigma_{\mathrm{tr}(\mathbf{D}^c)} = 1.8 \times 10^{-3} \|\mathbf{D}_2\|$$

$$\mathbf{L}_1 = \begin{bmatrix} 475 & 0 & 0 \\ 0 & 475 & 0 \\ 0 & 0 & -1000 \end{bmatrix} \frac{1}{s}$$ Random initial texture

$$\mu_{\mathrm{tr}(\mathbf{D}^c)} - \mathrm{tr}(\mathbf{D}_1) = -4.7 \times 10^{-3} \|\mathbf{D}_1\|$$
$$\sigma_{\mathrm{tr}(\mathbf{D}^c)} = 2.9 \times 10^{-3} \|\mathbf{D}_1\|$$

Los Alamos

NNSA

Dependence of L^c on Crystal Orientations

- Random initial texture

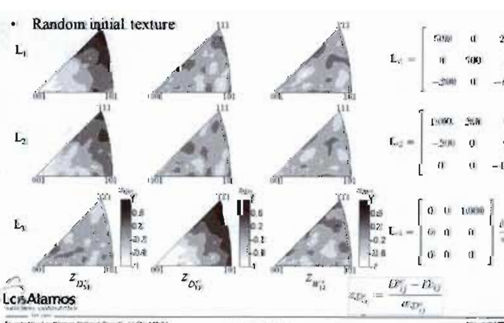

$$\mathbf{L}_1 = \begin{bmatrix} 500 & 0 & 200 \\ 0 & 500 & 0 \\ -200 & 0 & -1000 \end{bmatrix} \frac{1}{s}$$

$$\mathbf{L}_2 = \begin{bmatrix} 1000 & 200 & 0 \\ -200 & 0 & 0 \\ 0 & 0 & -1000 \end{bmatrix} \frac{1}{s}$$

$$\mathbf{L}_3 = \begin{bmatrix} 0 & 0 & 1000 \\ 0 & 0 & 0 \\ 0 & 0 & 0 \end{bmatrix} \frac{1}{s}$$

$$z_{D^c_{ij}} = \frac{D^c_{ij} - D_{ij}}{\sigma_{D^c_{ij}}}$$

Los Alamos

NNSA

CPFEM Analysis Conclusions

- $\mathbf{D}^c$ and $\mathbf{W}^c$ follow a normal distribution due to the crystal interactions.
- Their mean tensors are equal to the corresponding applied values and their $\mathrm{tr}(\mathbf{D}^c) \approx \mathrm{tr}(\mathbf{D})$ensors change with time
- Tr(Dc) = tr(D)
- $\mathbf{R}^c$ influences $\mathbf{D}^c$

Los Alamos

NNSA

III. 3-D Stochastic Polycrystal Plasticity Methods

Obtaining L^c with Stochastic Variation

- The CPFEM analysis results show that $\mathbf{L}^c$ follows a tensor normal distribution
- Engler (2002) and Ma et al. (2004) varied $\mathbf{D}^c$ according to a normal distribution and obtained an improved description of the polycrystal behavior
  - Hypothesis: Improvement is due to statistically representing the crystal interactions

Stochastic Mean-Field Polycrystal Methods

- Each $\mathbf{D}^{c\prime}$ is treated as a normally distributed random tensor $\mathbf{D}^{c\prime}$, $\mathrm{tr}(\mathbf{D}^c) = \mathrm{tr}(\mathbf{D})$, and $\mathbf{W}^c = \mathbf{W}$

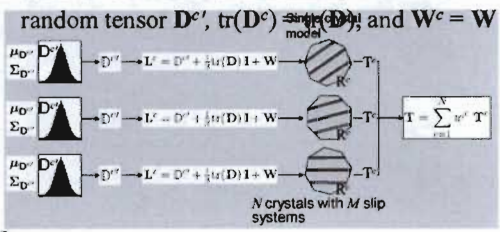

Engler (2002), Ma et al. (2004)

Single Crystal Model

- Kinematics

$$\mathbf{F}^c = \mathbf{F}^c_e\mathbf{F}_p = \mathbf{R}^c\mathbf{U}^c\mathbf{F}_p = \mathbf{R}^c(\mathbf{I} + \epsilon^c)\mathbf{F}_p \quad \|\epsilon^c\| \ll 1$$

$$\mathbf{D}^c = \mathbf{R}^c\dot{\epsilon}^c\mathbf{R}^{cT} + \mathbf{R}^c\mathbf{D}_p\mathbf{R}^{cT} + \mathbf{R}^c\epsilon^c\mathbf{W}_p\mathbf{R}^{cT} - \mathbf{R}^c\mathbf{W}_p\epsilon^c\mathbf{R}^{cT}$$

$$\mathbf{W}^c = \dot{\mathbf{R}}^c\mathbf{R}^{cT} + \mathbf{R}^c\mathbf{W}_p\mathbf{R}^{cT} + \mathbf{R}^c\epsilon^c\mathbf{D}_p\mathbf{R}^{cT} - \mathbf{R}^c\mathbf{D}_p\epsilon^c\mathbf{R}^{cT} - \frac{1}{2}\mathbf{R}^c(\epsilon^c\dot{\epsilon}^c - \dot{\epsilon}^c\epsilon^c)\mathbf{R}^{cT}$$

$$\dot{\mathbf{R}}^c = \mathbf{W}^c\mathbf{R}^c + \mathbf{R}^c\left[-\mathbf{W}_p^c - \epsilon^c\mathbf{D}_p^c + \mathbf{D}_p^c\epsilon^c + \frac{1}{2}(\dot{\epsilon}^c\epsilon^c - \epsilon^c\dot{\epsilon}^c)\right]$$

$$\mathbf{L}_p^c = \sum_{s=1}^{M}\dot{\gamma}^s\,\mathbf{b}_0^s \otimes \mathbf{n}_0^s \quad \mathbf{D}_p^c = \sum_{s=1}^{M}\dot{\gamma}^s\mathbf{m}_0^s \quad \mathbf{W}_p^c = \sum_{s=1}^{M}\dot{\gamma}^s\mathbf{q}_0^s$$

- D[illegible]

$$\dot{\gamma}^s = \dot{\gamma}^s(\tau^s) = \dot{\gamma}_0\exp\left[-\frac{F_0}{k\theta^c}\left\langle 1 - \left\langle\frac{|\tau^s| - \tau_0^s\frac{\mu}{\mu_0}}{\tau_0\frac{\mu}{\mu_0}}\right\rangle^{p}\right\rangle^{q}\right]\mathrm{sign}(\tau^s)$$

$$\mathbf{T}^c = 2\mu(\theta^c)\left(\mathbf{R}^c\epsilon^c\mathbf{R}^{cT} - \mathbf{R}^c\mathbf{A}(\theta^c - \theta_0)\mathbf{R}^{cT}\right) + \lambda(\theta^c)\,\mathrm{tr}(\epsilon^c - \mathbf{A}(\theta^c - \theta_0))\,\mathbf{I}$$

$$\tau^s = 2\mu(\theta^c)\,\mathbf{m}_0^s \cdot \epsilon^c$$

State Variables

- C[illegible] $\mathbf{R}^c$

$$\mathbf{R}_t^c = \exp(\mathbf{W}^c\Delta t)\mathbf{R}_{t-\Delta t}^c\exp\left(\left(-\mathbf{W}_p^c - \epsilon_t^c\mathbf{D}_p^c + \mathbf{D}_p^c\epsilon_t^c + \frac{1}{2}(\dot{\epsilon}^c\epsilon_t^c - \epsilon_t^c\dot{\epsilon}^c)\right)\Delta t\right)$$

- Slip system flow [illegible] τ_0^s

$$h_{\alpha\beta} = [r + (1 - r)\delta_{\alpha\beta}]\,h_\beta \qquad h_\beta = h_0\left(\frac{s_s^\beta - \tau_0^\beta}{s_s^\beta - \tau_{0}}\right)$$

$$s_s^\beta = s_s^\beta(\dot{\gamma}, \theta^c) = s_{s0}\left(\frac{\dot{\gamma}}{\dot{\gamma}_0}\right)^{\frac{k\theta^c}{A}}$$

$$\dot{\theta}^c = \frac{\eta}{\rho c_p}\sum_{s=1}^{N}\tau^s\dot{\gamma}^s$$

- Crystal temperature θ^c

Kok et al. (1996), Acharya and Beaudoin (2000), Kocks (1976)

Deviatoric Symmetric Random Tensors

- Since is $\mathbf{D}^{c\prime}$ is deviatoric and symmetric, it is re[illegible] $d_i^{c\prime} = \mathbf{V}_i \cdot \mathbf{D}^{c\prime}$ by $\mathbf{D}^{c\prime} = \sum_{i=1}^{5} d_i^{c\prime}\mathbf{V}_i$ or $\mathbf{d}^{c\prime}$
- The $\mathbf{d}^{c\prime}$ covariance matrix is sy[illegible] th[illegible] [illegible]pendent c[illegible]

$$\Sigma_{\mathbf{D}^{c\prime}} = \sum_{i=1}^{5}\sum_{j=1}^{5}(\Sigma_{\mathbf{d}^{c\prime}})_{ij}\mathbf{V}_i \otimes \mathbf{V}_j$$

$$\mathbf{V}_1 = \frac{1}{\sqrt{2}}(\mathbf{e}_1 \otimes \mathbf{e}_1 - \mathbf{e}_2 \otimes \mathbf{e}_2)$$

$$\mathbf{V}_2 = -\frac{1}{\sqrt{6}}(\mathbf{e}_1 \otimes \mathbf{e}_1 + \mathbf{e}_2 \otimes \mathbf{e}_2) + \sqrt{\frac{2}{3}}\mathbf{e}_3 \otimes \mathbf{e}_3$$

$$\mathbf{V}_3 = \frac{1}{\sqrt{2}}(\mathbf{e}_2 \otimes \mathbf{e}_3 + \mathbf{e}_3 \otimes \mathbf{e}_2)$$

$$\mathbf{V}_4 = \frac{1}{\sqrt{2}}(\mathbf{e}_1 \otimes \mathbf{e}_3 + \mathbf{e}_3 \otimes \mathbf{e}_1)$$

$$\mathbf{V}_5 = \frac{1}{\sqrt{2}}(\mathbf{e}_1 \otimes \mathbf{e}_2 + \mathbf{e}_2 \otimes \mathbf{e}_1)$$

Distribution of $D^{c'}$

- The PDF of $D^{c'}$ is
  $$f_{D''}(D'') = \frac{1}{4\pi^2\sqrt{2\pi \det \Sigma_{D''}}} \exp\left(-\frac{1}{2}(D'' - \mu_{D''}) \cdot \Sigma_{D''}^{-1}(D'' - \mu_{D''})\right)$$
  $$\Sigma_{D''} = \sum_{i=1}^{5} \sigma_i^2 \, \Phi_i \otimes \Phi_i$$
- U $\Sigma_{D''}^{-1} = \sum_{i=1}^{5} \frac{1}{\sigma_i^2} \Phi_i \otimes \Phi_i$ position
  $$\det \Sigma_{D''} = \prod_{i=1}^{5} \sigma_i^2$$

Los Alamos

NNSA

Assigning the Covariance Tensor

- We simplify the assignment of the $\mathbf{D}^{c'}$ covariance by assuming it is isotropic
- T $\Sigma_{d''} = 2\sigma_n^2 \mathbf{I}_5$ nce is defined by a single p $\Sigma_{D''} = 2\sigma_n^2 \mathcal{S} - \frac{2}{3}\sigma_n^2 \mathbf{I} \otimes \mathbf{I}$ $\qquad \mathcal{S}\mathbf{A} = \frac{1}{2}(\mathbf{A} + \mathbf{A}^T)$
  - σ_n^2
  - where
- We also assume is constant with time

Los Alamos

NNSA

Standard Normal Tensor

- The random tensor $\mathbf{N}'$ is defined by the random vector $\mathbf{n}'$ $\quad \mu_{n'} = 0 \quad \Sigma_{n'} = \mathbf{I}_5$
- $\mathbf{n}'$ has the mean $\quad f_{n'}(n'') = \frac{1}{2\pi^2\sqrt{2\pi}} \exp\left(-\frac{1}{2} n'' \cdot n''\right)$ and covariance matrix
  - $d^{c'} = \Sigma_{d''}^{\frac{1}{2}} n^{c'} + \mu_{d''}$
- A realization of the random $\Sigma_{d''}^{\frac{1}{2}} = \sqrt{2}\sigma_n \mathbf{I}_5$ transformed into the realization of the vector $\mathbf{d}^{c'}$ according to
  - When the $\mathbf{D}^{c'}$ covariance is isotropic,

Los Alamos

NNSA

Stochastic Taylor Model (STM)

- The random tensor $\mathbf{D}^{c'}$ is defined by $\Sigma_{D''} = 2\sigma_n^2 \mathcal{S} - \frac{2}{3}\sigma_n^2 \mathbf{I} \otimes \mathbf{I}$
  - $\mu_{D^{c'}} = \mathbf{D}'$
  - $d^{c'}(t) = \sqrt{2}\sigma_n n^{c'} + d'(t) \qquad \mathbb{D}^{c'} = \sum_{i=1}^{5} d_i^{c'} \mathbf{V}_i$
- The realizations are calculated from
  - $\mathcal{R}^c(\epsilon_c^t) = -\mathbf{R}^{cT}\mathbb{D}_c'\mathbf{R}^c + \frac{1}{\Delta t}(\epsilon_c^t - \epsilon_{c,\Delta t}^t) + \sum_{s=1}^{M} \dot{\gamma}^s (\mathbf{m}_s^c + \epsilon_c^t \mathbf{q}_s^c - \mathbf{q}_s^c \epsilon_c^t) = 0$
- Crystal residual equation solved with Newton-Raphson
  $$\epsilon_c = \epsilon_c' + \frac{1}{3}\mathrm{tr}(\epsilon_c)\mathbf{I} = \epsilon_c' + \frac{1}{3}\mathrm{tr}\left(\int_{t-\Delta t} \dot{\epsilon}\, dt\right)\mathbf{I}$$
  $$\approx \epsilon_c' + \frac{1}{3}\left(\mathrm{tr}(\epsilon_{t-\Delta t}) + \mathrm{tr}(\mathbf{D}_c)\Delta t\right)\mathbf{I}.$$

Los Alamos

NNSA

STM Schematic

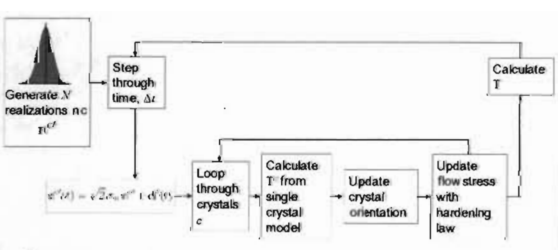

Los Alamos

NNSA

STM Sensitivity to Variance Value

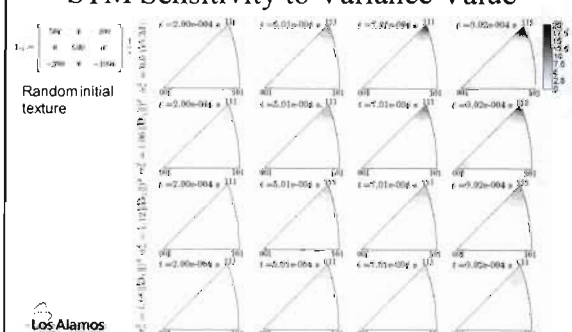

Los Alamos

NNSA

No-Constraints Model (NCM)

- Ensures stress equilibrium by assuming $\mathbf{T}^c = \mathbf{T}$
- Solves for $\mathbf{D}^{c\prime}$ and $\mathbf{T}'$ with a sparse, non-linear solver

$$\mathcal{R}^{\prime}(\epsilon_t^{\prime}) = -\mathbf{R}^{\prime}\mathbf{D}_t^{\prime}\mathbf{R}^{\prime} + \frac{1}{\Delta t}(\epsilon_t^{\prime} - \epsilon_{t-\Delta t}^{\prime}) + \sum_{s=1}^{N} \dot{\gamma}^s(\mathbf{m}_0^s + \epsilon_t^{\prime}\mathbf{q}_0^s - \mathbf{q}_0^s\epsilon_t^{\prime}) = 0$$

$$\mathcal{R}^{\prime\prime}(\mathbf{D}^{\prime}) = -\mathbf{D}^{\prime} + \sum_{c=1}^{N} w^c\mathbf{D}^{c\prime} = 0 \qquad \epsilon_t^{\prime}(\mathbf{T}^{\prime}) = \frac{1}{2\mu(\theta_t)}\mathbf{R}^{\prime\,-1}\mathbf{T}^{\prime}\mathbf{R}^{\prime}$$

- The $\mathbf{D}^{c\prime}$ predicted by the NCM describe, to a degree, the influence of $\mathbf{R}^c$ on $\mathbf{D}^{c\prime}$

Los Alamos

NNSA

Stochastic No-Constraints Method (SNCM)

- The random tensor $\mathbf{D}^{c\prime}$ is defined by

$$\Sigma_{\mathbf{D}^{c\prime}} = 2\sigma_n^2\,\mathcal{S} - \frac{2}{3}\sigma_n^2\,\mathbf{I}\otimes\mathbf{I}$$

$$\mu_{\mathbf{D}^{c\prime}} = \mathbf{D}^{\prime} + \alpha_s\Delta\mathbf{D}^{c\prime} \qquad \Delta\mathbf{D}^{c\prime} = \mathbf{D}^{c\prime} - \mathbf{D}^{\prime}$$

where

$$\mathrm{d}^{c\prime}(t) = \sqrt{2}\,\sigma_n\,\mathrm{n}^{c\prime} + \mu_{\mathrm{d}^{c\prime}}(t)$$

is calculated with the NCM

- The $\mathbf{T}^c$ are calculated from the resultant $\mathbf{L}^c$ in the same manner as in the STM.

Los Alamos

NNSA

SNCM Schematic

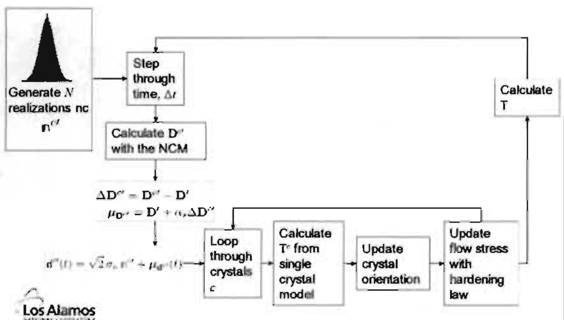

Los Alamos

NNSA

SNCM Sensitivity to α_s

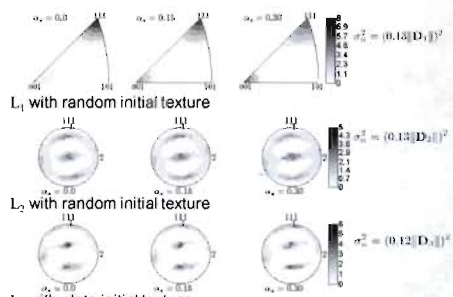

Los Alamos

NNSA

Experimental Calibration and Validation

- Upset forgings of P/M and rolled Tantalum cylinders
- Powder metallurgy (P/M)
  - Random initial texture
  - Three cylinders loaded to ε = -0.5, ε = -1.0, and ε = -2.0, respectively
- As-rolled bar
  - Two cylinders loaded to ε = -1.0 and ε = -2.0

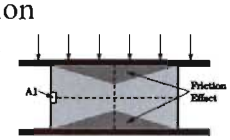

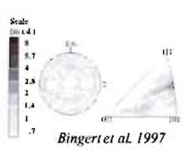

Bingert et al. 1997

Los Alamos

NNSA

Calibration and Validation of STM and SNCM

- Calibration: Determination of σ_n^2 and α_s to match measured P/M textures
- Validation: Comparisons of predicted textures to the as-rolled bar textures
- We also predict the texture using the FCM and VPSC to provide bench marks
  - In the VPSC simulation, the rotation of each crystal is coupled with the ratio of one neighbor crystal, chosen randomly

Los Alamos

NNSA

Calibration Using P/M Forging Results

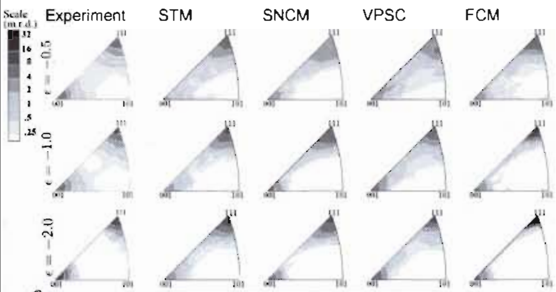

$\sigma_n^2 = (0.11\|\mathbf{D}\|)^2 \quad \alpha_s = 0.2$

Validation with As-rolled Bar Forging Results

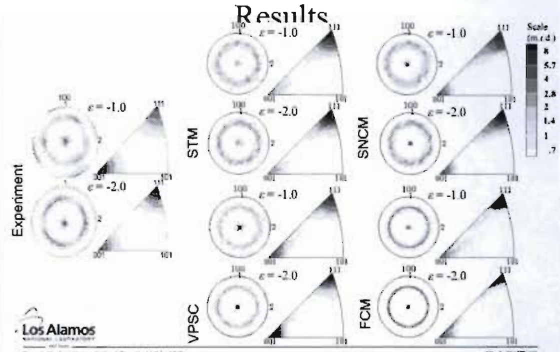

Computational Expense

- STM less accurate than SNCM and VPSC but more efficient

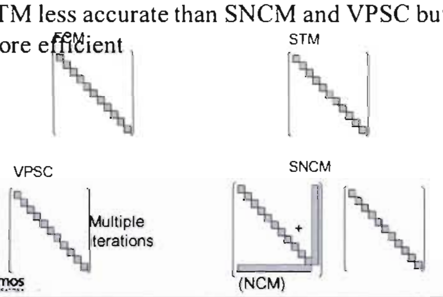

Stochastic Model Conclusions

- The STM is more accurate than the FCM and only slightly more computationally expensive.
- The SNCM is more accurate than the STM but three times more computationally expensive
  - As accurate as the VPSC

IV. Tantalum Taylor Specimen Analysis

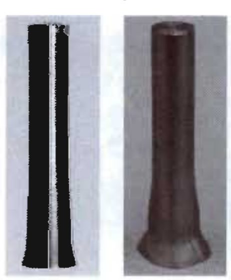

Taylor Impact Test

- A cylindrical specimen is fired at hardened steel anvil at a high velocity
- Plastic strain rates range from 10^4 s^{-1} to 0 s^{-1}
- A large range of textures occurs along the specimen

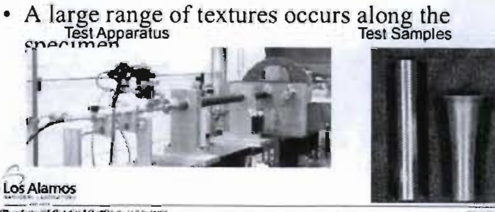

Taylor (1946, 1948)

Summary of Taylor Specimen Study

- We compare the responses of two tantalum Taylor impact specimens
  - Powder metallurgy specimen (P/M) specimen with equiaxed crystals and a random initial texture
  - Round-c[...]r square rolled (RCSR) specimen with an asym[...] crystals (30:1 ratio)

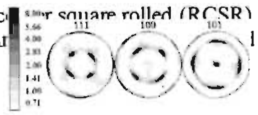

- We also model the experiments using the STM in an FE simulation

Discrete Representation of Initial Textures

- The ODF measured using X-ray diffraction

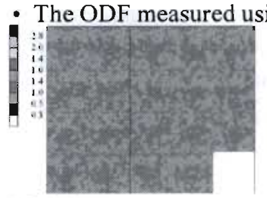

P/M texture

- 1000 weighted orientations are extracted

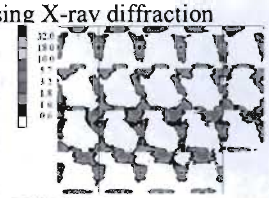

RCSR texture

Kocks (1990)

Experiment Details

- Specimens are 30 caliber and 2.0 in long
- Deformed using Helium-gas driven gun at LANL
- Impact in medium vacuum (1.3 KPa or 10 Torr)
- Projectiles recovered after the test
- Initial ve[...]r timing system
  - P/M sp[...]
  - RCSR [...]

Finite Element (FE) Simulation

- Specimens represented with 3-D mesh of 5,620 nodes and 23,328 tetrahedral elements
- Impact simulated with EPIC-06
  - Explicit time stepping scheme
  - Lagrangian kinematic description
- We [...] friction and

Material Model

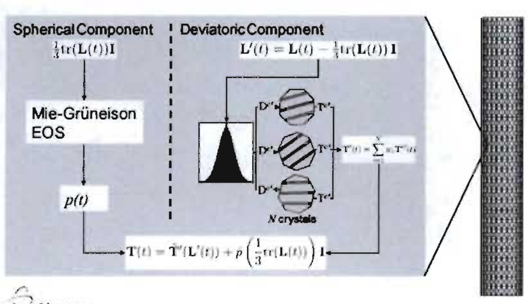

Zel'dovich and Raizer (1967), Walsh et al. (1957)

Initial Orientation Assignment

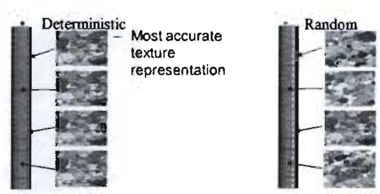

- Random assignment retards the texture evolution.
- The retardation effect increases with decreasing N

Beaudoin et al. (1993)

Determining the Value of N

- Computational cost is high
  - 23,328×N non-linear crystal solutions are conducted at each time step
  - 23,328×28×N state variables are stored
- Investigate sensitivity of material model to N
  - One time step, $dt = 10\ \mu s$
  - Average of 10 STM simulations
- Ev^{err} $= \frac{|\sigma_{e0} - \sigma_{eN}|}{\sigma_{e0}}$ ror and ODF error compared $\begin{bmatrix} 500 & 0 & 0 \\ 0 & 500 & 0 \\ 0 & 0 & -1000 \end{bmatrix}$ to $err_{f(R)} = \frac{\int |f(R_0^c) - f(R_N^c)|\, dR^c}{\int |f(R_0^c)|\, dR^c}$ entations

Los Alamos

Operated by Los Alamos National Security, LLC for NNSA LA-UR-10-03X28 NNSA

Sensitivity of the Model Accuracy to N

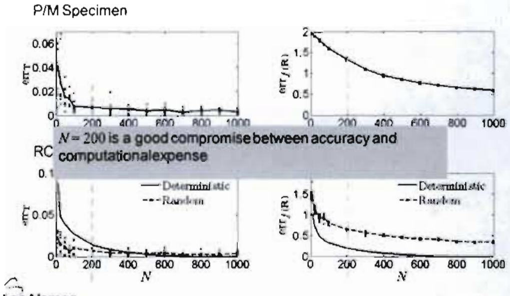

Los Alamos

Operated by Los Alamos National Security, LLC for NNSA LA-UR-10-03X28 NNSA

Simulation Details

- Both specimen impacts are simulated with the measured initial velocities for 110 μs
- The model parameters τ_{0_0} and h_0 vary for the P/M and RCSR specimens
  - No data available to determine values
  - We determine the values by fitting the predicted deformed lateral cross-section of the specimens to the P/M: $\tau_{0_0} = 0.075$ GPa, $h_0 = 3.5$ GPa; RCSR: $\tau_{0_0} = 0.05$ GPa, $h_0 = 3.5$ GPa

Los Alamos

Operated by Los Alamos National Security, LLC for NNSA LA-UR-10-03X28 NNSA

Recovered Specimens

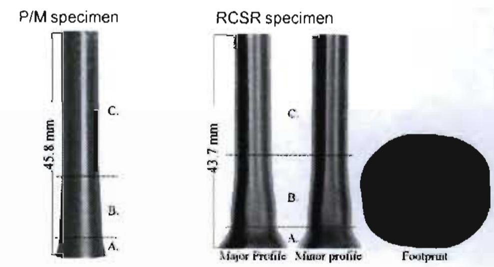

Los Alamos

Operated by Los Alamos National Security, LLC for NNSA LA-UR-10-03X28 NNSA

Predicted P/M Specimen Deformation

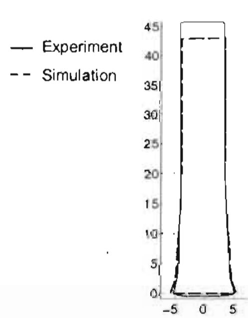

Los Alamos

Operated by Los Alamos National Security, LLC for NNSA LA-UR-10-03X28 NNSA

Predicted RCSR Specimen Deformation

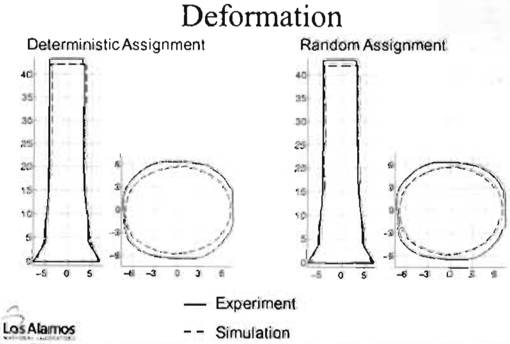

Los Alamos

Operated by Los Alamos National Security, LLC for NNSA LA-UR-10-03X28 NNSA

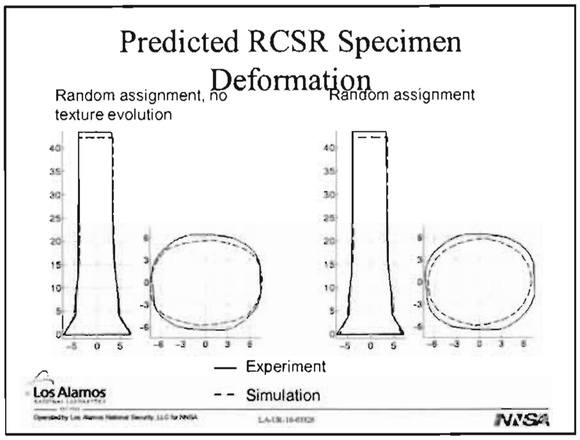
Predicted RCSR Specimen Deformation
Random assignment, no texture evolution
Random assignment
Experiment
Simulation
Los Alamos

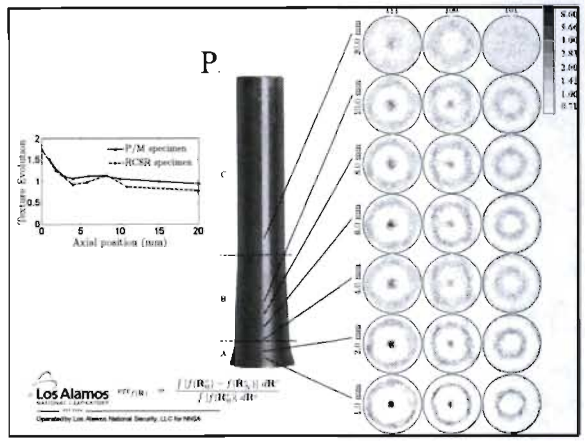
P/M specimen
RCSR specimen
Texture Evolution
Axial position (mm)
Los Alamos

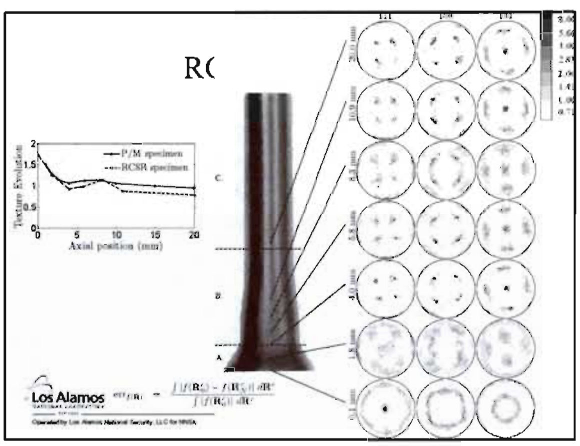
P/M specimen
RCSR specimen
Texture Evolution
Axial position (mm)
Los Alamos

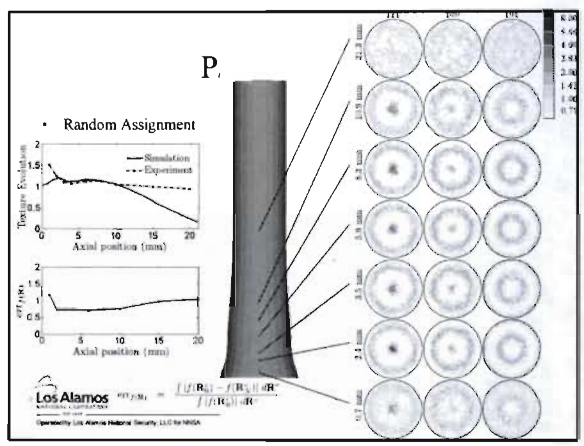
Random Assignment
Simulation
Experiment
Texture Evolution
Axial position (mm)
Axial position (mm)
Los Alamos

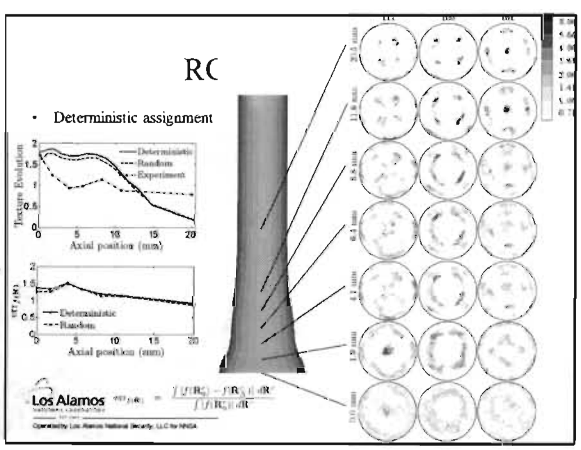
Deterministic assignment
Deterministic
Random
Experiment
Texture Evolution
Axial position (mm)
Deterministic
Random
Axial position (mm)
Los Alamos

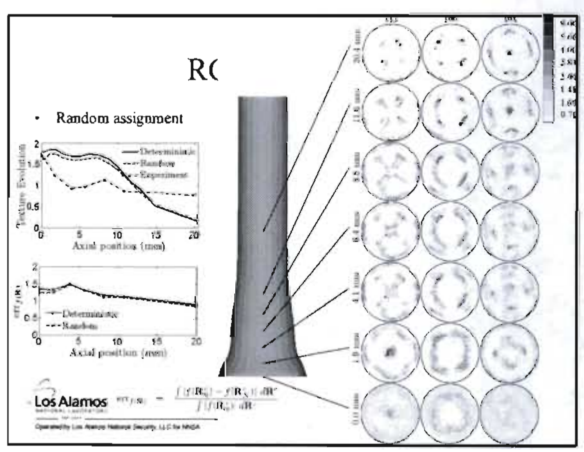
Random assignment
Deterministic
Random
Experiment
Texture Evolution
Axial position (mm)
Deterministic
Random
Axial position (mm)
Los Alamos

FCM vs. STM

- We repeat the P/M specimen simulation using the FCM
- The STM provides a 16.2% increase in accuracy with a 17.9% increase in computational time

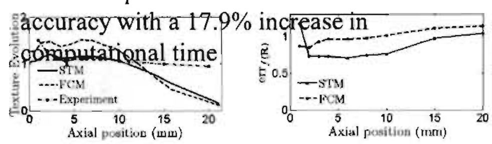

Los Alamos

Effect of Initial Texture on Specimen Deformation

- Initial texture affects the shape of the footprint but not the general shape of the lateral cross-section

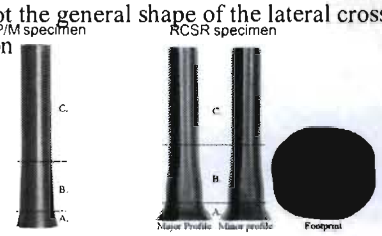

Los Alamos

Local Minimum in the Texture Evolution

- Why local minimum in the texture evolution at 4 mm?

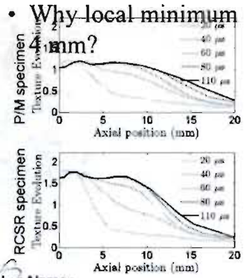

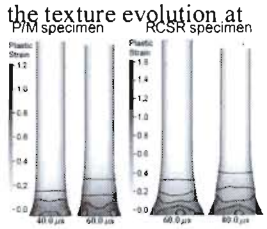

Simulations using random selection

Los Alamos

RCSR Specimen Texture Evolution

- The RCSR specimen texture is resistant to evolution
  - Resistance is not captured by our material model
- Resistance may be due to elongated crystals (30:1 ratio)
- Crystals can't rotate due to compatibility

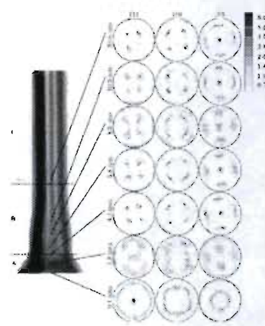

Los Alamos

Taylor Impact Analysis Conclusions

- The initial texture influences the deformed footprint, but not the deformed lateral cross-section
- The RCSR specimen resists evolution due to its elongated crystal morphology
- Our FE simulations accurately predict the P/M specimen behavior
- They do not accurately predict the RCSR specimen behavior because they do not account for the elongated morphology

Los Alamos

V. Future Work

- Analyze the convergence towards steady-state ODFs in more complex polycrystals
  - Conduct analyses similar to Kumar and Dawson (1996) and Kumar (1996) using the STM rather than the FCM
- Verify CPFEM results with realistic crystal shapes and non-uniform crystal sizes
- Develop relationship between σ^2 and the polycrystal material parameters and applied loading.
- Investigate the texture evolution resistance in the RCSR

Los Alamos

Questions?

Los Alamos

The ODF of the Planar Polycrystal

- Orientation Distribution Function (ODF)

Random Initial Texture $f_{\Theta_0}(\theta_0) = 1/\pi$

FCM $\Gamma(t) = \Gamma \quad \Lambda^c(t) = \Lambda \quad \Omega^c(t) = \Omega$

- $f_{\Theta^c}(\theta^c) = f_{\Theta_0}(\tilde{\theta}_0(\theta^c, \Gamma^c, \Lambda^c, \Omega^c)) \left|\partial_{\theta^c}\tilde{\theta}_0(\theta^c, \Gamma^c, \Lambda^c, \Omega^c)\right|$
- $f_{\Theta^c}(\theta^c) = \dfrac{\sec\theta^{c2}/\cosh(t\mathcal{F} - W)^2}{\pi\left(1 - \frac{(\Lambda\Lambda+\Omega\Gamma+\Omega)\tan\theta^c)^2}{\mathcal{F}^2}\right)\left(1 + \frac{(\Lambda\Lambda+\mathcal{F}\tanh(t\mathcal{F}-W))^2}{(\Lambda\Gamma+\Omega)^2}\right)}$

STM $= \dfrac{e^{-\frac{(x-\mu_\Gamma)^2}{2\sigma_\Gamma^2}}}{\sqrt{2\pi}\sigma_\Gamma} \quad f_\Lambda(y) = \dfrac{e^{-\frac{(y-\mu_\Lambda)^2}{2\sigma_\Lambda^2}}}{\sqrt{2\pi}\sigma_\Lambda} \quad \Omega^c(t) = \Omega$

- $f_{\Theta^c}(\theta^c) = \int_{-\infty}^{\infty}\int_{-\infty}^{\infty} f_{\Theta_0}(\tilde{\theta}_0(\theta^c, x, y, \Omega^c)) f_\Gamma(x) f_\Lambda(y) \left|\partial_{\theta^c}\tilde{\theta}_0(\theta^c, x, y, \Omega^c)\right| dx\, dy$

Los Alamos

Symmetric Random Variables

- A symmetric random tensor **X** can be represented as a 6-D random vector $\mathbf{x}$

$x_i = \mathbf{E}_i \cdot \mathbf{X} \quad \mathbf{X} = \sum_{i=1}^{6} x_i \mathbf{E}_i$

$\mathbf{E}_1 = \mathbf{e}_1 \otimes \mathbf{e}_1 \quad \mathbf{E}_4 = \frac{1}{\sqrt{2}}(\mathbf{e}_2 \otimes \mathbf{e}_3 + \mathbf{e}_3 \otimes \mathbf{e}_2)$

$\mathbf{E}_2 = \mathbf{e}_2 \otimes \mathbf{e}_2 \quad \mathbf{E}_5 = \frac{1}{\sqrt{2}}(\mathbf{e}_1 \otimes \mathbf{e}_3 + \mathbf{e}_3 \otimes \mathbf{e}_1)$

$\mathbf{E}_3 = \mathbf{e}_3 \otimes \mathbf{e}_3 \quad \mathbf{E}_6 = \frac{1}{\sqrt{2}}(\mathbf{e}_1 \otimes \mathbf{e}_2 + \mathbf{e}_2 \otimes \mathbf{e}_1)$

$\mu_x = \frac{1}{M}\sum_{m=1}^{M} \mathbf{x}_m \qquad \Sigma_x = \frac{1}{M}\sum_{m=1}^{M} (\mathbf{x}_m - \mu_x) \otimes (\mathbf{x}_m - \mu_x)$

– The 2nd-order mean tensor and 4th-order covariance tensor of x are $\mu_{\mathbf{X}} = \sum_{i=1}^{6} \mu_{x_i} \mathbf{E}_i$ and $\Sigma_{\mathbf{X}} = \sum_{i=1}^{6}\sum_{j=1}^{6} \Sigma_{x_{ij}} \mathbf{E}_i \otimes \mathbf{E}_j$

Los Alamos

Skew-Symmetric Random Variables

- A skew-symmetric random tensor **Y** can be represented as a 3-D random vector

$y_i = \mathbf{G}_i \cdot \mathbf{Y} \quad \mathbf{Y} = \sum_{i=1}^{3} y_i \mathbf{G}_i$

$\mathbf{G}_1 = \frac{1}{\sqrt{2}}(\mathbf{e}_2 \otimes \mathbf{e}_3 - \mathbf{e}_3 \otimes \mathbf{e}_2)$

$\mathbf{G}_2 = \frac{1}{\sqrt{2}}(\mathbf{e}_1 \otimes \mathbf{e}_3 - \mathbf{e}_3 \otimes \mathbf{e}_1)$

$\mathbf{G}_3 = \frac{1}{\sqrt{2}}(\mathbf{e}_1 \otimes \mathbf{e}_2 - \mathbf{e}_2 \otimes \mathbf{e}_1)$

$\mu_y = \frac{1}{M}\sum_{m=1}^{M} \mathbf{y}_m \qquad \Sigma_y = \frac{1}{M}\sum_{m=1}^{M} (\mathbf{y}_m - \mu_y) \otimes (\mathbf{y}_m - \mu_y)$

– The mean tensor and covariance tensor of y are $\mu_{\mathbf{Y}} = \sum_{i=1}^{3} (\mu_y)_i \mathbf{G}_i$ and $\Sigma_{\mathbf{Y}} = \sum_{i=1}^{3}\sum_{j=1}^{3} (\Sigma_y)_{ij} \mathbf{G}_i \otimes \mathbf{G}_j$

Los Alamos

Eigenvalue Differences From CPFEM Analysis

- $\mathbf{L}_1$
- $\mathbf{L}_2$
- $\mathbf{L}_3$

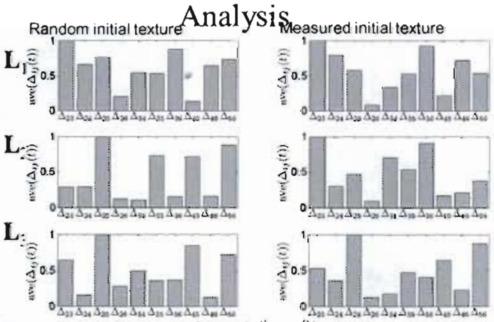

$\Delta_{ij} = |\sigma_i^2 - \sigma_j^2|$

Los Alamos

Powder Metallurgy (P/M) Specimen

- 30 caliber (7.62 mm diameter) and 50.8 mm long (2.0 in)

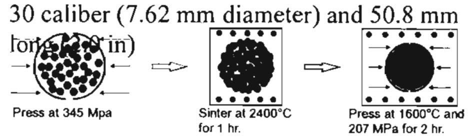

- Crystals are relatively equiaxed with a random initial texture

Los Alamos

Round-Corner Square Rolled (RCSR) Specimen

- .30 caliber (7.62 mm diameter) and 50.8 mm long (2.0 in)

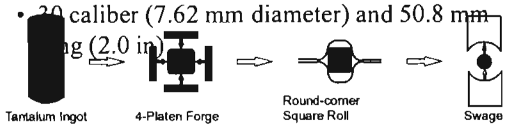

- Asymmetric ... crystals (30:1 ratio)

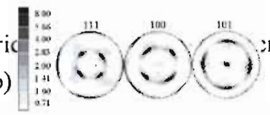

Micro-Structure Driven Yield Surface

- Maudlin et al. (2003) investigate the RCSR specimen by generating a yield surface
  - Use the FCM with 1000 crystals
- Found strong coupling between the normal and shear stresses
- Mixed-mode coupling produces a shearing deformation in the cross-section

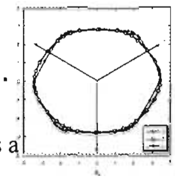

3-D Images of RCSR Specimen

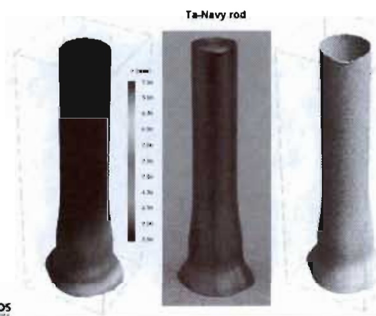

3-D Measurements of RCSR Radial Cross-section

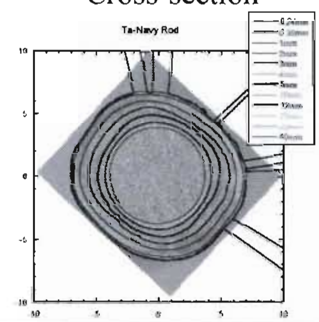

Deterministic vs. Random Assignment

- Differences are not sufficient to recommend either method

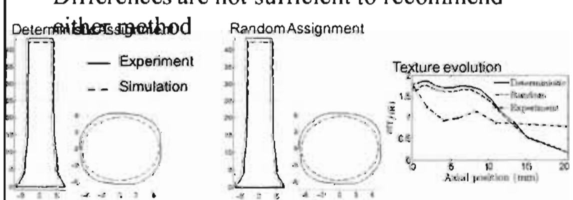

Mesh Convergence Study

- P/M Specimen with $N = 20$

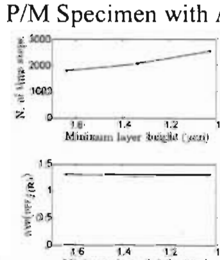

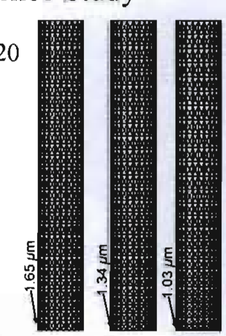

CPFEM Analyses Conclusions

- $\mathbf{D}^c$ and $\mathbf{W}^c$ follow normal distributions in planar and 3-D polycrystals

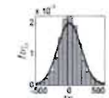

$tr(\mathbf{D}^c) \approx tr(\mathbf{D})$

- Since the elastic strain is small, $tr(\mathbf{D}^c) \approx tr(\mathbf{D})$

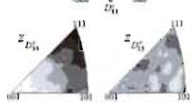

- The crystal orientations $\mathbf{R}^c$ influence the $\mathbf{D}^c$ components corresponding to the non-zero $\mathbf{D}$ components
- Future Work: Verify CPFEM results with realistic crystal shapes and non-uniform crystal sizes

Los Alamos

Stochastic Models for Approximating L^c

- $\mathbf{D}^{c\prime}$ sampled from tensor normal distributions
- $\mathbf{D}^{c\prime}$ is defined by a single, constant variance and a $\mu_{D^{c\prime}}$ = D'nsor $\mu_{D^{c\prime}} = \mathbf{D}' + \alpha \Delta \mathbf{D}^{c\prime}$
  - STM: SNCM:
- Computational Cost:

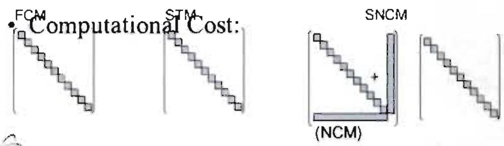

Los Alamos

Stochastic Models Accuracy

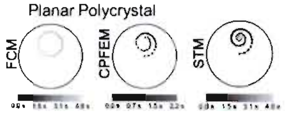

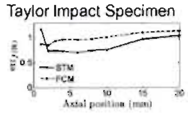

3-D Tantalum Compression Experiments

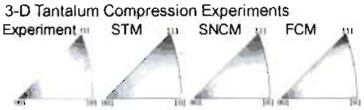

- **Future Work:** Develop relationship between σ^2 and the polycrystal material parameters and applied loading.

Los Alamos

Planar Polycrystal Analysis

- There is a link between texture evolution and the behavior of coupled oscillators as predicted by the Kuramoto model
- STM and CPFEM predict that the planar polycrystal texture always converges to a steady-state ODF
- **Future Work:** Analyze the convergence towards steady-state ODFs in more complex polycrystals

Kumar and Dawson (1996) and Kumar (1996)

Los Alamos

Tantalum Taylor Specimen Impact Study

- Initial texture of specimen affects the footprint but not the lateral cross-section
- RCSR specimen is resistant to texture evolution possibly due to its crystal morphology

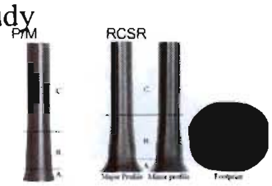

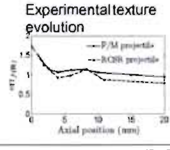

Los Alamos

Future Work for RCSR Tantalum Taylor Specimen

- Conduct experiments on RCSR samples at various strain rates.
- Simulate the deformation of an RCSR polycrystal using the CPFEM to validate our assumption that the elongated crystals resist rotation.
- Develop a mean-field polycrystal plasticity model that accounts for the elongated crystal morphology

Los Alamos